Electronic Supplementary Material (ESI) for Journal of Materials Chemistry A.

Supplementary Information

Title: Metal-organic framework modulated to site-isolate Cl$^{•}$ pendants via radical inter-conversion for degrading hard-to-ionize aqueous organic wastes

Authors: Minsung Kim,‡[ab] Md Al Mamunur Rashid,‡[a] Yun Jeong Choe,[a] Sang Hoon Kim,[a] Jung-Hyun Lee,[b] Keunhong Jeong,*[c] and Jongsik Kim*[d]

‡ contributed equally to this work.

* doas1mind@kma.ac.kr (K. Jeong); jkim40@khu.ac.kr (J. Kim).

Affiliations:

[a] Extreme Materials Research Center, Korea Institute of Science and Technology, Seoul, 02792, South Korea.

[b] Department of Chemical & Biological Engineering, Korea University, Seoul, 02841, South Korea.

[c] Department of Physics and Chemistry, Korea Military Academy, Seoul, 01805, South Korea.

[d] Department of Chemical Engineering, Kyung Hee University, Yongin, 17104, South Korea.

Table of Contents

Synthesis of 2-chlorobenzene-1,4-dicarboxylic acid

2-chlorobenzene-1,4-dicarboxylic acid (H_2BDC-Cl) was synthesized by following the procedures reported elsewhere.[1-3] 133.9 mmol of KOH (Daejung, 85.0 %) was dissolved in 150 mL of de-ionized H_2O, mixed with 32.5 mmol of 3-chloro-4-methylbenzoic acid (TCI Chemical, >98.0 %) and 99.0 mmol of $KMnO_4$ (Sigma-Aldrich, ≥99.0 %), stirred at 90 °C for 18 hours, cooled to 25 °C, and stirred at 25 °C for additional 18 hours. The resulting synthetic intermediate was filtered using Celite® 545 (Yakuri Pure) to isolate the filtrate, which in turn was diluted with 125 mL of de-ionized H_2O and acidified using HCl (J. T. Baker, 36.5-38.0 wt. % in H_2O) to adjust the pH value of the synthetic mixture to ~1.0.[1-3] This led to the generation of white precipitate.[1, 2] The white precipitate (H_2BDC-Cl) was then vacuum-filtered, rinsed with 1.0 L of de-ionized H_2O, and dried under vacuum (1.3×10^{-4} bar) at 25 °C for 18 hours.[1-3]

Synthesis of UiO-66 and UiO-66-Cl

UiO-66 and UiO-66-Cl were synthesized according to the protocols slightly modified based on those reported elsewhere.[4-6] Typically, 2.57 mmol of $ZrCl_4$ (Sigma-Aldrich, ≥99.9 %), 1.29 mmol of protonated organic strut (benzene-1,4-dicarboxylic acid (H_2BDC, Sigma-Aldrich, ≥98.0 %) for UiO-66; H_2BDC-Cl for UiO-66-Cl), and 90.04 mmol of dodecanoic acid (Daejung, ≥99.0 %) were mixed with 150 mL of N,N'-dimethyl formamide (DMF, Daejung, ≥99.5 %), loaded in a 200 mL Teflon acid digestion sleeve, heated at 120 °C for 48 hours, cooled to 25 °C, vacuum-filtered, and rinsed with 1.0 L of DMF.[4-6] 1.0 g of UiO-66 (or UiO-66-Cl) as-synthesized was then mixed with 450 mL of DMF and 2.25 mL of HCl, stirred at 90 °C for 12 hours to dissolve deprotonated dodecanoic acids (dodecanoates) clogging the pores of UiO-66 (or UiO-66-Cl), cooled to 25 °C, vacuum-filtered, and rinsed using 500 mL of DMF and 250 mL of $CHCl_3$ (Daejung, ≥99.5 %).[4-6] 2.0 g of UiO-66 (or UiO-66-Cl) subjected to the elimination of dodecanoates was finally immersed in 250 mL of $CHCl_3$ for three days, vacuum-filtered, rinsed using 250 mL of $CHCl_3$, situated inside in a custom-built stainless steel vessel, purged with a N_2 at 25 °C for 5 minutes, purged with a CO_2 at 25 °C for 5 minutes, exposed to super-critical CO_2 (SC-CO_2) environment (CO_2 pressure (P_{CO2}) of ~90 bar at 70-80 °C) for 5 minutes before a stainless steel vessel was depressurized to P_{CO2} of ~1 bar at 30-40 °C.[7] UiO-66 (or UiO-66-Cl) in a stainless steel vessel experienced SC-CO_2 extraction protocols (*vide supra*) ten times prior to its storage under vacuum (1.3×10^{-4} bar) at 25 °C.[6, 7]

Synthesis of Mn oxide-N and Fe oxide-S

Mn oxide-N and Fe oxide-S were synthesized according to the procedures we reported elsewhere.[8, 9] Typically, 20 mmol of $KMnO_4$ and 20 mmol of $MnCl_2•4H_2O$ (Sigma-Aldrich, ≥99.0 %) were dissolved in 200 mL of de-ionized H_2O, placed in a 250 mL Teflon acid digestion sleeve, stirred at 25 °C for half an hour, situated in a stainless steel reactor vessel, exposed to hydro-thermal synthetic conditions at 160 °C for 6 hours, and cooled to 25 °C.[8] The resulting Mn oxide (α-MnO_2) was collected via vacuum filtration, rinsed with 750 mL of de-ionized H_2O and 750 mL of ethanol (Daejung, 94.5 %), and dried at 90 °C for 18 hours.[8] 1.0 g of Mn oxide was then loaded in a quartz tube and put inside a tube furnace prior to being exposed to a N_2-balanced gas stream consisting of 5,000 ppm NO and 3 vol. % O_2 at 150 °C for an hour with a ramping rate of 10 °C min^{-1} and a total flow rate of 500 mL min^{-1}.[8] This resulted in the formation of Mn oxide-N.[8] Meanwhile, 20 mmol of $FeSO_4•7H_2O$ (Sigma-Aldrich, ≥99.0 %) and 20 mmol of $C_2H_2O_4•2H_2O$ (oxalic acid dihydrate, Junsei, 99.5-100.2 %) were dissolved in 100 mL of de-ionized H_2O, stirred at 50 °C for half an hour, isolated via vacuum filtration, rinsed with 500 mL of de-ionized H_2O and 500 mL of ethanol, dried at 70 °C for 18 hours, and calcined at 300 °C for an hour with a ramping rate of 5 °C min^{-1}.[8, 10] The resulting iron oxide was then loaded in a quartz tube and put inside a tube furnace prior to being exposed to a N_2-balanced gas stream consisting of 500 ppm SO_2 and 3 vol. % O_2 at 500 °C for an hour with a ramping rate of 10 °C min^{-1} and a total flow rate of 500 mL min^{-1}. This resulted in the formation of Fe oxide-S.[9]

Characterizations

X-ray diffraction (XRD) patterns of UiO-66/UiO-66-Cl were acquired on a D8 Advance (Bruker) using monochromatic Cu K_α radiation (wavelength of 1.54 Å) with analytic conditions of a step size and a scan speed of 0.02° per step and 2 seconds per step, respectively. Field emission-scanning electron microscope (FE-SEM) images of UiO-66/UiO-66-Cl were acquired on a Regulus 8230 (Hitachi) at 15 kV. Energy-dispersive X-ray spectroscopy (EDX) mapping images of UiO-66/UiO-66-Cl were acquired on a Ultim max 170 (Oxford) at 15 kV. High resolution transmission electron microscopy (HRTEM) images of UiO-66/UiO-66-Cl were acquired on a Titan 80-300^{TM} (FEI) at 300 keV. Bulk elemental compositions of UiO-66/UiO-66-Cl were assessed via elemental analysis (EA) on a FLASH 2000 (Thermo Fisher Scientific). Elemental compositions and phases of UiO-66/UiO-66-Cl surfaces were investigated via X-ray photoelectron (XP) spectroscopy on a PHI 5000 Versa Probe (Ulvac-Phi), whose resolution was 0.05 eV. XP spectra of UiO-66/UiO-66-Cl at the Zr 3d, C 1s, O 1s, N 1s, or Cl 2p regimes were curve-fitted using Gaussian and Lorentzian functions alongside with the utilization of an adventitious carbon band centered at binding energy of ~284.5 eV as a reference to correct binding energies of surface phases for UiO-66/UiO-66-Cl. Concentrations of aqueous Zr/Mn/Fe/S, Cl, and N species present in reaction solutions were quantified via inductively coupled plasma (ICP) on an ICS 3000 (Thermo Fisher Scientific), ion chromatography on an 883 basic IC Plus (Metrohm), and total organic nitrogen (TN) on a TN analyzer (Shimadzu), respectively. Background-subtracted, *in situ* diffuse reflectance infrared Fourier transform (DRIFT) spectra of UiO-66/UiO-66-Cl under dry/wet NH_3 streams were acquired on an FT/IR/is20 (Thermo Fisher Scientific), a KBr optics, and a mercury-cadmium-telluride (MCT) detector, all of which were coupled to provide the resolution of 4 cm^{-1} and allowed for the protocols depicted in Fig. 3 caption.[6, 11] A BELSORP-MAX (MicrotracBEL Corp.) served to acquire H_2O isotherms of UiO-66/UiO-66-Cl at 20-40 °C (Fig. S7), whereas a NOVA 2200e (Quantachrome Instruments) served to acquire N_2 isotherms (Fig. S4) and CO/CO_2 isotherms of UiO-66/UiO-66-Cl (Fig. S10-S11) at -196 °C and at -20-20 °C, respectively.[6, 8, 12] Typically, UiO-66/UiO-66-Cl were degassed under vacuum (~3.0 X 10^{-6} bar) at 150 °C for 3 hours prior to the collection of their $H_2O/N_2/CO/CO_2$ isotherms, whereas surface areas of UiO-66/UiO-66-Cl accessible to $H_2O/N_2/CO/CO_2$ were assessed via Brunauer-Emmett-Teller (BET) theory with the consideration of the amounts of $H_2O/N_2/CO/CO_2$ adsorbed on the surfaces at partial pressure (P/P_0) range of 0.05-0.30.[6, 8, 12-14] In addition, N_2-accessible meso-pore volumes (V_{MESO}) and micro-pore volumes (V_{MICRO}) of UiO-66/UiO-66-Cl were evaluated using Barrett-Joyner-Halenda (BJH) and t-plot theories, respectively, or using NLDFT theory with the presumption that the pores of UiO-66/UiO-66-Cl are featured by and similar to slit-shaped pores of carbons.[6, 15] In addition, $H_2O/CO_2/CO$ isotherms of UiO-66/UiO-66-Cl were simulated using Toth equation (Eqn. S1), where $N_{H2O/CO2/CO}$ and A denote the number of $H_2O/CO_2/CO$ adsorbed in a per-gram of UiO-66 (or UiO-66-Cl) and maximum number of $H_2O/CO_2/CO$ adsorbed in a per-gram of UiO-66 (or UiO-66-Cl), respectively.[6, 8, 11-14] Moreover, B, C, and P denote the constant, constant associated with surface heterogeneity, and pressure, respectively.[6, 8, 11-14] (See the details in Table S5, S8, and S9.) Isosteric heats of $H_2O/CO_2/CO$ adsorption for UiO-66 (or UiO-66-Cl) at near-zero coverages of $H_2O/CO_2/CO$ served to evaluate the binding strengths between the surface and $H_2O/CO_2/CO$ via Clausius-Clapeyron equation (Eqn. S2), in which P_A/P_B and R denote the pressures (bar) at the temperatures of T_A/T_B (K) and ideal gas constant (8.3145 J mol^{-1} K^{-1}), respectively.[6, 8, 11-14]

$$N_{H2O}(or\ N_{CO}/N_{CO2}) = \mathrm{A} \times \frac{B \times P}{(1 + (B \times P)^{C})^{(\frac{1}{C})}} \quad (S1)$$

$$ln\left(\frac{P_A}{P_B}\right) = \frac{E_{H2O}\ (or\ E_{CO}/E_{CO2})}{R} \times \left(\frac{T_A - T_B}{T_A \times T_B}\right) (S2)$$

Electron paramagnetic resonance (EPR) spectra of reaction mixtures/solutions were collected on an EMX-plus (Bruker), for which 5,5-dimethyl-1-pyrroline N-oxide (DMPO) served as a spin trapping agent of $^{\bullet}$OH, $^{\bullet}$OOH, $O_2^{\bullet -}$, or Cl$^{\bullet}$ (oxidized Cl functionality of UiO-66-Cl) under analytic conditions that a center magnetic field was 3435 G, a resonance frequency was 9.64 GHz, a modulation frequency was 100 kHz, a microwave power was 2.95 mW, a modulation amplitude was 1 G, a sweep width was 120 G, and a sweep time was 48 seconds.[6, 8, 12] The resulting EPR spectra of reaction mixtures/solutions were simulated using EasySpin (version 5.2.28) and spectral parameters (Table S10), with which the EPR spectra were curve-fitted using Gaussian and Lorentzian functions to diagnose relative abundance of DMPO-OH, DMPO-OOH, HDMPO-OH, and DMPO-X adducts.[6, 8, 12] (See the details in Fig. S13 and Table S11.) CO-pulsed chemisorption experiments of the materials were performed on a BELCAT II (Microtrac MRB) at 40 °C.[7-10, 12] An ultra-performance liquid chromatography (UPLC;

Acquity, Waters) equipped with a mass spectrometry (MS; G2, Synapt) and a BEH C18 column (1.7 µm; 2.1X100.0 mm; Acquity, Waters) served to collect LC-MS spectra of reaction solutions under analytic conditions of a flow rate of 0.2 mL min^{-1}, an injection volume of 5 µL, and a mobile phase A/B of de-ionized H_2O/CH_3OH (A:B=4:6).[6] A MS served to detect reaction intermediates in negative mode electro-spray ionization (ESI) with a source temperature, a desolvation temperature, a cone gas flow, and a desolvation gas flow of 120 °C, 350 °C, 100 L hr^{-1}, and 800 L hr^{-1}, respectively.[6]

Structural elucidation of UiO-66 and UiO-66-Cl

An AVANCE III HD 400 (Bruker) served to validate the successful synthesis of $H_2BDC\text{-}Cl$ (Fig. S1) and to quantify the number of DMF coordinated to μ_3-OH (Y) present in the base unit of defective UiO-66 ($Zr_6(\mu_3\text{-}O)_4(\mu_3\text{-}OH)_4(BDC)_{6\text{-}X}[(H_2O)(OH)]_{2X}\bullet(DMF)_Y$) or UiO-66-Cl ($Zr_6(\mu_3\text{-}O)_4(\mu_3\text{-}OH)_4(BDC\text{-}Cl)_{6\text{-}X}[(H_2O)(OH)]_{2X}\bullet(DMF)_Y$) in tandem with the number of dodecanoates clogging the pores of defective UiO-66 or UiO-66-Cl via ^1H-nuclear magnetic resonance (^1H-NMR) spectroscopy.[6, 16, 17] Typically, 10 mg of UiO-66 (or UiO-66-Cl) was digested using 0.06 mL of aqueous HF (Fisher Scientific, 48.0 wt. % in H_2O), mixed with 0.54 mL of dimethyl sulfoxide-d_6 (DMSO-d_6, Cambridge Isotope Laboratories, 99.9 %) functioning as a NMR solvent, and subjected to ^1H-NMR spectroscopy experiment.[6] The molar amount of DMF (Y) or dodecanoate relative to that of BDC (6-X) (or BDC-Cl (6-X)) strut inherent to defective UiO-66 (or UiO-66-Cl) was evaluated using Eqn. S3-S6, where •/•• (purple), 2 (red), I (green), and III (blue) indicate integrated value of protons for DMF, dodecanoates, BDC, and BDC-Cl, respectively,[6, 16, 17] as illustrated in Fig. S5 and Table S2.

$$molar\ amount\ of\ DMF\ relative\ to\ that\ of\ BDC = \frac{4H}{area\ of\ '\mathrm{I}'} \times \frac{area\ of\ '\bullet'\ or\ '\bullet\bullet'}{3H} \quad (S3)$$

$$molar\ amount\ of\ DMF\ relative\ to\ that\ of\ BDC - Cl = \frac{1H}{area\ of\ '\mathrm{III}'} \times \frac{area\ of\ '\bullet'\ or\ '\bullet\bullet'}{3H} \quad (S4)$$

$$molar\ amount\ of\ (deprotonated)\ dodecanoic\ acid\ relative\ to\ that\ of\ BDC = \frac{4H}{area\ of\ '\mathrm{I}'} \times \frac{area\ of\ '2'}{16H} \quad (S5)$$

$$molar\ amount\ of\ (deprotonated)\ dodecanoic\ acid\ relative\ to\ that\ of\ BDC - Cl = \frac{1H}{area\ of\ '\mathrm{III}'} \times \frac{area\ of\ '2'}{16H} \quad (S6)$$

A Titrando 848 Plus (Metrohm) served to quantify the number of missing organic struts (X) present in the base unit of defective UiO-66 or UiO-66-Cl via titration.[18] Typically, mortar and pestle were used to grind UiO-66 (or UiO-66-Cl), whose 50 mg was mixed with 60 mL of 0.01 mol $NaNO_3$ (Sigma-Aldrich, ≥99.0 %) dissolved in 1.0 L of de-ionized H_2O (0.01 M $NaNO_3$), stirred at 25 °C for 18 hours, subjected to the pH adjustment to 3.0 with the use of HCl, and titrated using 0.1 mol of NaOH (Daejung, ≥97.0 %) dissolved in 1.0 L of de-ionized H_2O (0.1 M NaOH) up to the pH value of ~11.0 with an injection volume of 0.025 mL and an injection rate of 0.02 mL min^{-1}.[18] Titration experiments speculate that the elimination of an organic strut (BDC or BDC-Cl) from intact UiO-66 (or UiO-66-Cl) base unit can generate four Zr^{4+} sites, where two H_2O and two OH^- can be adsorbed to produce Zr^{4+}-H_2O and Zr^{4+}-OH analogues, respectively.[18] In addition, it was hypothesized that protons (H^+) of μ_3-OH, Zr^{4+}-H_2O, and Zr^{4+}-OH can be released from defective UiO-66 (or UiO-66-Cl) base unit upon the elevation of pH values in the order of $\mu_3\text{-}OH \rightarrow Zr^{4+}\text{-}H_2O \rightarrow Zr^{4+}\text{-}OH$, whereas all the protons (H^+) liberated can be utilized to equilibrate with OH^- of 0.1 M NaOH added at three equivalent points.[18] Of note, plot of the 1st derivative of the pH value with respective to the volume of 0.1 M NaOH fed ($d(pH)/d(V_{NaOH})$) versus V_{NaOH} can be curve-fitted using Lorentzian function to provide three bands with V_{NaOH} values centered at 5.4-5.5 mL (peak I), 7.0-7.5 mL (peak II), and 9.3-9.4 mL (peak III), at which pH values indicate equivalent points of defective UiO-66 (or UiO-66-Cl).[18] (See the details in Fig. 2, Fig. S6, and Table S3.) In addition to the construction of the relationship between X and Y for defective UiO-66 (or UiO-66-Cl) using ^1H-NMR spectroscopy experiments (Table S4),[6, 16, 17] the difference of V_{NaOH} values for peak I and peak III can serve to obtain X value of defective UiO-66 (or UiO-66-Cl) according to Eqn. S7-S8.[18]

$$\frac{V_{NaOH,peak\,III}(mL) - V_{NaOH,peak\,I}(mL)}{50\ X\ 10^{-3}\ g\ of\ UiO-66\ (or\ UiO-66-Cl)} \times \frac{1\ L}{1000\ mL} \times \frac{0.1\ mol\ of\ OH^-}{1\ L} = \frac{6 \times X\ (mol)}{50\ X\ 10^{-3}\ g\ of\ UiO-66\ (or\ UiO-66-Cl)} \quad (S7)$$

$$\frac{6 \times X\ (mol)}{50\ X\ 10^{-3}\ g\ of\ UiO-66\ (or\ UiO-66-Cl)} = \frac{moles\ of\ titrated\ protons\ innate\ to\ base\ unit\ for\ UiO-66\ (or\ UiO-66-Cl)\ in\ terms\ of\ X}{weight\ (g)\ of\ base\ unit\ for\ UiO-66\ (or\ UiO-66-Cl)\ in\ temrs\ of\ X} \quad (S8)$$

Overall, X/Y values acquired via titration/^{1}H-NMR spectroscopy experiments did serve to elucidate the base unit of defective UiO-66 or UiO-66-Cl, as specified in Table S4.

Computations

All the calculations were performed using Gaussian 16 software[19] along with the utilization of density functional theory (DFT) level of M-06L (meta-GGA functional),[20] which was reported to successfully compute UiO-66 surface.[21] This was because meta-GGA functional includes implicit parameterization of non-covalent interaction energies, thus enabling reliable computations for open-shell *3d* metal systems.[22] In addition, the basis set of def2svp for C, H, O, Cl atoms[23] and that of Stuttgart-Dresden SDD for Zr atom[24] were used due to their inclusion of effective core potential and associated pseudo-potentials with Grimme correction, whereas integrals were evaluated via density-fitting schemes automatically generated to improve computational efficiency. Furthermore, auto-fitting was implemented for the basis sets, whereas ultra-fine grid was exploited for two electron integrals with symmetry being turned off via external command. To compute reaction free energies in aqueous environments, solvent effect was considered using solvation model of density (SMD) with water as a solvent.[25] The SMD model calculates the change in Gibbs free energy of species *i* ($\Delta G_{solvation,\ i}$) involved in its phase transition from gas-phase to liquid-phase (solvent) upon the consideration of electrostatic and cavitation dispersion energies, thus making the SMD model well-suited to compute aqueous phase free energies.[26] The SMD model is a continuum solvation model based on quantum mechanical charge density of a solute molecule interacting a solvent with continuum description, while full electron density is used without defining partial atomic charges. Hence, the SMD model is widely adaptable to charged/uncharged solute molecules in a host of solvents, for which a few key descriptors such as dielectric constant, refractive index, bulk surface tension, and acidity/basicity are known.[25] Reaction free energy (ΔE) is defined in Eqn. S9, where ε_0 and G_{CORR} indicate total electronic energy and correction term to Gibbs free energy because of internal energy for reactant or product.[6]

$$\Delta E = \sum (\varepsilon_0 + G_{CORR})_{PRODUCTS} - \sum (\varepsilon_0 + G_{CORR})_{REACTANTS} \quad (S9)$$

In this study, ΔE values were calculated using restricted/unrestricted DFT for closed/open shell systems. Geometry optimizations of the reactants/products were performed in the gas phase and subsequently in the solvent phase. To ensure that the geometries computed are featured by minimum energies, harmonic frequency analysis was performed at the same level of theory. All stationary points in the potential energy surface were proven to be global minima. (No imaginary frequency was found in the frequency calculation.) Of note, our main focus was to inspect the viability of radical transfer from $^{\bullet}$OH to Cl functionality of BDC-Cl struts for UiO-66-Cl. In this regard, UiO-66-Cl structure was simplified to an BDC-Cl strut coordinated to four Zr atoms for saving computational expense.[27] BDC-Cl structure was initially constructed by substituting H atom of BDC with Cl atom. Meanwhile, four Zr atoms of the simplified UiO-66-Cl structure were frozen in an aqueous media throughout the structural optimizations and/or energy calculations. Of additional note, spin contamination may be problematic in unrestricted quantum chemical calculations (*i.e.*, the artificial mixing of different electronic spin states). DFT models are generally less sensitive to spin contamination than Hartree-Fock ones. To ensure that spin contamination had little effect on the calculations, spin contamination was assessed by analyzing the deviation of $<S^2>$ values to the exact values (0.75 for a doublet).[28] The deviations were <10 % for all the species, confirming that spin contamination was insignificant throughout the calculations on the reaction pathways.[29]

Reactions

0.2 g of UiO-66 (or UiO-66-Cl) was added to 100 mL of de-ionized H_2O, stirred at 300 rpm and 25 °C for 5 minutes, and mixed with 30 mmol of H_2O_2 (Daejung, 30 wt. % in H_2O) for the initiation of H_2O_2 dissection run at 300 rpm and 25 °C. 0.7 mL of reaction aliquot was taken away from reaction mixture per 10 minutes, quenched using 1 µL of methanol (Sigma-Aldrich, ≥99.8 %), filtered with 0.45 µm-sized PES syringe filter (Whatman®), and mixed with $CuSO_4 \bullet 5H_2O$ (Sigma-Aldrich, ≥98.0 %), neocuproine ($C_{14}H_{12}N_2$, Sigma-Aldrich, ≥98.0 %), and phosphate buffer (Samchun, pH of 7.2) to analyze H_2O_2 concentration via $C_{14}H_{12}N_2$ method, whose procedures were specified in our previous studies.[6, 8-10, 12, 30, 31] Conversion of H_2O_2 (X_{H2O2}) was assessed using Eqn. S10, where $C_{H2O2,\,0}$ and C_{H2O2} denotes initial H_2O_2 concentration and H_2O_2 concentration at a specific reaction time, respectively.[6, 8-10, 12, 30, 31]

$$X_{H2O2}\ (\%) = \frac{C_{H2O2,0}\ (mol_{H2O2}\ L^{-1}) - C_{H2O2}\ (mol_{H2O2}\ L^{-1})}{C_{H2O2,0}\ (mol_{H2O2}\ L^{-1})} \times 100 \quad (S10)$$

Initial H_2O_2 dissection rate of UiO-66 (or UiO-66-Cl) in a per-Lewis acidic (LA) site basis ($-r_{H2O2,\,0,\,LA}$) or in a per-Brönsted acidic (BA) site basis ($-r_{H2O2,\,0,\,BA}$) was assessed using Eqn. S11-S12, where k_{APP} and $N_{H2O2,\,0}$ denote apparent reaction rate constant (slopes of -ln ($C_{H2O2}/C_{H2O2,\,0}$) versus time in Table S12) and initial amount of H_2O_2, respectively,[6, 8-10, 12, 30, 31] whereas numbers of LA/BA sites with effective CO_2 accessibilities contained in a per-gram of UiO-66 (or UiO-66-Cl) are specified in Table S7.

$$-r_{H2O2,0,LA}\ (min^{-1}) = \frac{k_{APP}\ (min^{-1}) \times N_{H2O2,0}\ (mol_{H2O2})}{number\ of\ LA\ sites\ included\ per\ 0.2\ g\ of\ UiO-66\ (or\ UiO-66-Cl)\ \ (mol_{LA})} \quad (S11)$$

$$-r_{H2O2,0,BA}\ (min^{-1}) = \frac{k_{APP}\ (min^{-1}) \times N_{H2O2,0}\ (mol_{H2O2})}{number\ of\ BA\ sites\ included\ per\ 0.2\ g\ of\ UiO-66\ (or\ UiO-66-Cl)\ \ (mol_{BA})} \quad (S12)$$

On the other hand, 0.2 g of UiO-66 (or UiO-66-Cl) was added to 100 mL of de-ionized H_2O containing 0.1 mmol of nitrobenzene (Sigma-Aldrich ≥99.0 %), phenol (Daejung, ≥99.0 %), phenol-d_6 (C_6D_5OD, Sigma-Aldrich, 99.0 atom % D), or aniline (Sigma-Aldrich, ≥98.0 %), stirred at 300 rpm and 25 °C for 5 minutes, and mixed with 30 mmol of H_2O_2 for the initiation of typical pollutant degradation run at 300 rpm and 25 °C, unless otherwise noted in the figure captions. 1.0 mL of reaction aliquot was taken away from reaction mixture per 10 minutes, quenched using 1 µL of methanol, filtered with 0.45 µm-sized PES syringe filter to analyze pollutant concentration via reverse-phase high performance liquid chromatography (HPLC) method, whose protocols were also detailed in our previous studies.[6, 8-10, 12, 30, 31] Conversion of pollutant ($X_{POLLUTANT}$) was assessed using Eqn. S13, where $C_{POL,\,0}$ and C_{POL} denotes initial pollutant concentration and pollutant concentration at a specific reaction time, respectively.[6, 8-10, 12, 30, 31]

$$X_{POLLUTANT}\ (\%) = \frac{C_{POL,0}\ (mol_{POLLUTANT}\ L^{-1}) - C_{POL}\ (mol_{POLLUTANT}\ L^{-1})}{C_{POL,0}\ (mol_{POLLUTANT}\ L^{-1})} \times 100 \quad (S13)$$

Initial pollutant degradation rate of UiO-66 (or UiO-66-Cl) in a per-Lewis acidic (LA) site basis ($-r_{POLLUTANT,\,0,\,LA}$) or in a per-Brönsted acidic (BA) site basis ($-r_{POLLUTANT,\,0,\,BA}$) was assessed using Eqn. S14-S15, where k_{APP} and $N_{POL,\,0}$ denote apparent reaction rate constant (slopes of -ln ($C_{POL}/C_{POL,\,0}$) versus time in Table S12) and initial amount of pollutant, respectively.[6, 8-10, 12, 30, 31]

$$-r_{POLLUTANT,0,LA}\ (min^{-1}) = \frac{k_{APP}\ (min^{-1}) \times N_{POL,0}\ (mol_{POLLUTANT})}{number\ of\ LA\ sites\ included\ per\ 0.2\ g\ of\ UiO-66\ (or\ UiO-66-Cl)\ \ (mol_{LA})} \quad (S14)$$

$$-r_{POLLUTANT,0,BA}\ (min^{-1}) = \frac{k_{APP}\ (min^{-1}) \times N_{POL,0}\ (mol_{POLLUTANT})}{number\ of\ BA\ sites\ included\ per\ 0.2\ g\ of\ UiO-66\ (or\ UiO-66-Cl)\ \ (mol_{BA})} \quad (S15)$$

In addition, initial pollutant degradation rate in a per-gram of UiO-66 (or UiO-66-Cl) was assessed using Eqn. S16.[6, 8]

$$-r_{POLLUTANT,0}\ (mol_{POLLUTANT}\ g_{CAT}^{-1}\ min^{-1}) = \frac{k_{APP}\ (min^{-1}) \times N_{POL,0}\ (mol_{POLLUTANT})}{0.2\ g\ of\ UiO-66\ (or\ UiO-66-Cl)} \quad (S16)$$

Energy barrier ($E_{BARRIER}$) and LA or BA site-directed pre-exponential factor ($k_{APP,\,0,\,LA}$ or $k_{APP,\,0,\,BA}$) of UiO-66 (or UiO-66-Cl) in decomposing phenol were assessed using Arrhenius plot of ln ($-r_{PHENOL,\,0,\,LA}$) versus 1/T (Eqn. S17) or ln (-$r_{\text{PHENOL, 0, BA}}$) versus 1/T (Eqn. S18), where T stands for reaction temperature.[6, 8, 12]

$$ln\left(-r_{PHENOL,0,LA}\right) = \underbrace{ln\left(k_{APP,0,LA} \times C_{PHENOL,0}\right)}_{y-intercept} + \underbrace{\frac{-E_{BARRIER}}{R}}_{slope} \times \left(\frac{1}{T}\right) \quad (S17)$$

$$ln\left(-r_{PHENOL,0,BA}\right) = \underbrace{ln\left(k_{APP,0,BA} \times C_{PHENOL,0}\right)}_{y-intercept} + \underbrace{\frac{-E_{BARRIER}}{R}}_{slope} \times \left(\frac{1}{T}\right) \quad (S18)$$

Aniline or pharmaceutical compound (acetaminophen (TCI Chemicals, >98.0 %), sulfanilamide (TCI Chemicals, >99.0 %), or sulfamethoxazole (SMX, TCI Chemicals, >98.0 %)) was subjected to degradation using the identical protocols to those utilized to degrade phenol (*vide supra*), except for altering the amount of aqueous contaminant from 0.1 mmol to 0.007 mmol. Initial degradation rate of aniline or pharmaceutical compound on UiO-66 (or UiO-66-Cl) in a per-Lewis acidic (LA) site basis (-$r_{\text{PHARMA, 0, LA}}$) was assessed using Eqn. S19, where k_{APP} and $N_{\text{PHARMA, 0}}$ denote apparent reaction rate constant (slopes of -ln ($C_{\text{PHARMA}}/C_{\text{PHARMA, 0}}$) versus time in Table S12) and initial amount of aniline (or pharmaceutical compound), respectively.[6, 8-10, 12, 30, 31]

$$-r_{PHARMA,0,LA}\,(min^{-1}) = \frac{k_{APP}\,(min^{-1}) \times N_{PHARMA,0}\,(mol_{PHARMA})}{number\ of\ LA\,sites\ included\ per\ 0.2\,g\ of\ UiO-66\ (or\ UiO-66-Cl)\ (mol_{LA})} \quad (S19)$$

Table S1. Textural and compositional properties of UiO-66 and UiO-66-Cl.

		UiO-66	UiO-66-Cl
$S_{\mathrm{BET,\ N2}}$ [a, b] ($\mathrm{m_{N2}}^{2}\ \mathrm{g_{CAT}}^{-1}$)		878.14 (± 17.31)	464.57 (± 18.64)
$V_{\mathrm{MICRO,\ N2}}$ [a, c] ($\mathrm{cm_{N2}}^{3}\ \mathrm{g_{CAT}}^{-1}$)		0.29 (± 0.04)	0.19 (± 0.01)
$V_{\mathrm{MESO,\ N2}}$ [a, d] ($\mathrm{cm_{N2}}^{3}\ \mathrm{g_{CAT}}^{-1}$)		0.17 (± 0.06)	0.22 (± 0.08)
$V_{\mathrm{PORE,\ N2}}$ [a, e] ($\mathrm{cm_{N2}}^{3}\ \mathrm{g_{CAT}}^{-1}$)		0.46 (± 0.07)	0.41 (± 0.08)
meso-porosity [f]		0.37 (± 0.14)	0.54 (± 0.22)
$S_{\mathrm{NLDFT,\ N2}}$ [a, g] ($\mathrm{m_{N2}}^{2}\ \mathrm{g_{CAT}}^{-1}$)		652.98 (± 5.57)	424.24 (± 39.71)
$V_{\mathrm{MICRO,\ NLDFT,\ N2}}$ [a, g] ($\mathrm{cm_{N2}}^{3}\ \mathrm{g_{CAT}}^{-1}$)		0.30 (± 0.01)	0.20 (± 0.01)
$V_{\mathrm{MESO,\ NLDFT,\ N2}}$ [a, g] ($\mathrm{cm_{N2}}^{3}\ \mathrm{g_{CAT}}^{-1}$)		0.26 (± 0.01)	0.14 (± 0.02)
$V_{\mathrm{PORE,\ NLDFT,\ N2}}$ [a, e] ($\mathrm{cm_{N2}}^{3}\ \mathrm{g_{CAT}}^{-1}$)		0.56 (± 0.01)	0.34 (± 0.02)
meso-porosity [f]		0.46 (± 0.02)	0.41 (± 0.06)
N/C [h]	calculated [i]	0.02 (<± 0.01)	0.03 (<± 0.01)
	observed [j]	0.04 (± 0.01)	0.03 (± 0.01)
	observed [k]	0.02 (± 0.01)	0.03 (± 0.01)
Cl/C [h]	calculated [i]	-	0.12 (<± 0.01)
	observed [k]	-	0.11 (± 0.01)
N/Zr [h]	calculated [i]	0.17 (<± 0.01)	0.17 (<± 0.01)
	observed [k]	0.17 (± 0.02)	0.18 (± 0.02)
C/Zr [h]	calculated [i]	6.84 (± 0.16)	6.68 (± 0.16)
	observed [k]	7.12 (± 0.03)	6.95 (± 0.32)
Cl/Zr [h]	calculated [i]	-	0.77 (± 0.02)
	observed [k]	-	0.73 (± 0.07)

[a] via N_2 physisorption. (See Fig. S4.) [b] via BET. [c] via t-plot. [d] via BJH. [e] $V_{\mathrm{MICRO}} + V_{\mathrm{MESO}}$. [f] V_{MESO} divided by V_{PORE}. [g] via NLDFT (N_2 at -196 °C on carbon with slit-shaped pores). [h] molar ratio. [i] via base unit. [j] via EA. [k] via XP spectroscopy.

Table S2. Compositions of DMF and dodecanoate relative to that of BDC (or BDC-Cl) for UiO-66 or (UiO-66-Cl).

	UiO-66	UiO-66-Cl
BDC	1	-
BDC-Cl	-	1
DMF	0.20 (± 0.01) [a]	0.22 (± 0.01) [a]
(deprotonated) dodecanoic acid	0.02 (<± 0.01) [a]	0.01 (<± 0.01) [a]

[a] via ^{1}H-NMR. (See Fig. S5.)

Table S3. Equivalent points of UiO-66 and UiO-66-Cl subjected to titration with the use of NaOH as a titrant.

	equivalent point		
	peak I (H^+ of μ_3-OH)	peak II (H^+ of H_2O on Zr^{4+}-H_2O)	peak III (H^+ of OH on Zr^{4+}-OH)
	UiO-66		
1st [a]	5.31	7.85	9.54
2nd [b]	5.90	7.89	9.45
3rd [c]	5.38	6.60	9.23
average	5.53 (± 0.26)	7.45 (± 0.60)	9.41 (± 0.13)
reference	5.44 (± 0.04) [18]	7.56 (± 0.01) [18]	9.51 (± 0.08) [18]
	UiO-66-Cl		
1st [d]	5.16	6.86	9.07
2nd [e]	5.47	7.38	9.42
3rd [f]	5.66	6.73	9.30
average	5.43 (± 0.21)	6.99 (± 0.28)	9.26 (± 0.15)

[a] See Fig. 2D. [b] See Fig. S6A. [c] See Fig. S6C. [d] See Fig. 2E. [e] See Fig. S6B. [f] See Fig. S6D.

Table S4. Numbers of missing organic strut (X) and DMF coordinated to μ$_3$-OH (Y) for UiO-66 or UiO-66-Cl.

UiO-66 (base unit of $Zr_6(\mu_3\text{-}O)_4(\mu_3\text{-}OH)_4(BDC)_{6\text{-}X}[(H_2O)(OH)]_{2X}\bullet(DMF)_Y$) [a, b]		
X [c]	1.068 (± 0.051)	
Y (DMF) [d]	BDC:DMF = (6-X):Y = 1:0.2; Y = 1.20-0.20X	0.62 (<± 0.01) mmol g_{CAT}^{-1}
Lewis acidic site (LA) [e]	2X	1.34 (± 0.07) mmol g_{CAT}^{-1}
Brönsted acidic site (BA)	4-Y+2X; 2.8+2.2X	3.23 (± 0.09) mmol g_{CAT}^{-1}
base unit [c, d, e]	1597.15 (± 7.39) g BASE UNIT^{-1}	
UiO-66-Cl (base unit of $Zr_6(\mu_3\text{-}O)_4(\mu_3\text{-}OH)_4(BDC\text{-}Cl)_{6\text{-}X}[(H_2O)(OH)]_{2X}\bullet(DMF)_Y$) [a, b]		
X [f]	1.373 (± 0.113)	
Y (DMF) [d]	BDC-Cl:DMF = (6-X):Y = 1:0.22; Y = 1.32-0.22X	0.59 (± 0.01) mmol g_{CAT}^{-1}
Lewis acidic site (LA) [e]	2X	1.60 (± 0.15) mmol g_{CAT}^{-1}
Brönsted acidic site (BA)	4-Y+2X; 2.68+2.22X	3.33 (± 0.18) mmol g_{CAT}^{-1}
Cl_{SUP} (or Cl^-_{SUP})	6-X	2.69 (± 0.03) mmol g_{CAT}^{-1}
base unit [d, e, f]	1719.26 (± 20.36) g BASE UNIT^{-1}	

[a] presuming that the removal of an organic strut (BDC or BDC-Cl) from UiO-66 or UiO-66-Cl can produce four open Zr^{4+} sites, where two H_2O and two OH^- are hypothetically adsorbed. [b] BDC: $C_8H_4O_4$; BDC-Cl: $C_8H_3O_4Cl$; DMF: C_3H_7NO. [c] via titration of UiO-66 using NaOH (X of 1.040, 1.025, and 1.140 in Fig. 2D, S6A, and S6C). [d] via ^{1}H-NMR of digested UiO-66 or UiO-66-Cl. (See Fig. S5.) [e] assuming that H_2O molecules on Zr^{4+}-H_2O sites are desorbed. [f] via titration of UiO-66-Cl using NaOH (X of 1.495, 1.223, and 1.400 in Fig. 2E, S6B, and S6D).

Table S5. Coefficients used to simulate H_2O isotherms for UiO-66 and UiO-66-Cl.

temperature (°C)	coefficient	UiO-66	UiO-66-Cl
20	A [a, b] ($mmol_{H2O}$ g_{CAT}^{-1})	23102.95	3067.86
	B [a, b] (bar^{-1})	0.01	0.04
	C [a, b] (dimensionless)	0.19	0.21
30	A [a, b] ($mmol_{H2O}$ g_{CAT}^{-1})	2737.61	379.56
	B [a, b] (bar^{-1})	0.02	0.12
	C [a, b] (dimensionless)	0.34	1.37
40	A [a, b] ($mmol_{H2O}$ g_{CAT}^{-1})	90.40	84.46
	B [a, b] (bar^{-1})	0.41	0.38
	C [a, b] (dimensionless)	0.58	0.55
20	$S_{BET, H2O}$ [a, c] (m_{H2O}^2 g_{CAT}^{-1})	506.7 (± 72.1)	441.2 (± 38.4)
	N_{H2O} [a, d] ($mmol_{H2O}$ g_{CAT}^{-1})	28.6	36.4
	S_{H2O} [a, e] (X10^3 m_{H2O}^2 mol_{H2O}^{-1})	17.7 (± 2.5)	12.1 (± 1.1)

[a] See Fig. S7. [b] via Toth fitting at $0<P/P_0<0.45$. [c] via BET at $0.05 \leq P/P_0 \leq 0.30$. [d] moles of H_2O adsorbed at P/P_0 of ~1.0. [e] $S_{BET, H2O}$ divided by N_{H2O}.

Table S6. Binding energies and concentrations of surface phases observed in XP spectra of UiO-66 and UiO-66-Cl.

		UiO-66	UiO-66-Cl
	Zr 3d domain [a, b]		
Zr 3d $_{5/2}$	binding energy (eV)	182.7	182.7
	concentration (%)	56.4	59.3
Zr 3d $_{3/2}$	binding energy (eV)	185.1	185.1
	concentration (%)	43.6	40.7
	C 1s domain [a, c]		
C-C/C-H	binding energy (eV)	284.6	284.6
	concentration (%)	67.2	58.4
C-N	binding energy (eV)	286.0	286.0
	concentration (%)	4.5	3.6
C-Cl	binding energy (eV)	-	286.6
	concentration (%)	-	12.9
C-O	binding energy (eV)	287.0	287.0
	concentration (%)	11.1	11.2
O-C=O	binding energy (eV)	288.8	288.8
	concentration (%)	17.2	13.9
	O 1s domain [a, d]		
Zr-O-Zr	binding energy (eV)	530.1	530.1
	concentration (%)	21.1	23.9
Zr-OH	binding energy (eV)	531.5	531.5
	concentration (%)	28.1	30.4
Zr-O-C	binding energy (eV)	531.9	531.9
	concentration (%)	38.6	34.8
H_2O [e]	binding energy (eV)	532.6	532.6
	concentration (%)	7.0	8.7
O-C=O	binding energy (eV)	533.8	533.8
	concentration (%)	5.2	2.2
	N 1s domain [a, f]		
C-N	binding energy (eV)	400.7	400.7
	concentration (%)	100	100
	Cl 2p domain [a, g]		
anionic Cl (Cl^-_{SUP}) 2p $_{3/2}$ [h]	binding energy (eV)	-	198.0
	concentration (%)	-	63.4
anionic Cl (Cl^-_{SUP}) 2p $_{1/2}$ [h]	binding energy (eV)	-	199.4
	concentration (%)	-	63.6
neutral Cl (Cl_{SUP}) 2p $_{3/2}$ [i]	binding energy (eV)	-	200.3
	concentration (%)	-	36.6
neutral Cl (Cl_{SUP}) 2p $_{1/2}$ [i]	binding energy (eV)	-	201.9
	concentration (%)	-	36.4

[a] via Gaussian and Lorentzian fittings; resolution of 0.05 eV. [b] See Fig. S8A. [c] See Fig. S8B. [d] See Fig. S9A. [e] H_2O on Zr^{4+}-H_2O. [f] See Fig. S9B. [g] See Fig. S9C. [h] Cl with ionic feature. [i] Cl with covalent feature.

Table S7. Quantification of surface sites available to homolytic H_2O_2 scission and/or $^{\bullet}OH \rightarrow Cl^{\bullet}_{SUP}$ for UiO-66 and UiO-66-Cl.

		UiO-66	UiO-66-Cl
	site accessible to CO [a]		
total calculated [b] ($mmol_{CO}\ g_{CAT}^{-1}$)		1.34 (± 0.07)	1.60 (± 0.15)
total observed [c] ($mmol_{CO}\ g_{CAT}^{-1}$; N_{CO})		0.08 (± 0.01)	0.07 (<± 0.01)
	site accessible to CO_2 [d]		
total calculated [b] ($mmol_{CO2}\ g_{CAT}^{-1}$)		5.18 (± 0.11)	8.22 (± 0.24)
total observed [e] ($mmol_{CO2}\ g_{CAT}^{-1}$; N_{CO2})		0.99 (± 0.05)	1.28 (± 0.01)
Lewis acidic site (LA)	calculated [b] ($mmol_{CO2}\ g_{CAT}^{-1}$)	1.34 (± 0.07)	1.60 (± 0.15)
	ratio (%)	25.8 (± 1.5)	19.5 (± 1.9)
	predicted [f] ($mmol_{CO2}\ g_{CAT}^{-1}$)	0.26 (± 0.02)	0.25 (± 0.02)
Brönsted acidic site (BA)	calculated [b] ($mmol_{CO2}\ g_{CAT}^{-1}$)	3.23 (± 0.09)	3.33 (± 0.18)
	ratio (%)	62.3 (± 2.1)	40.6 (± 2.5)
	predicted [f] ($mmol_{CO2}\ g_{CAT}^{-1}$)	0.62 (± 0.04)	0.52 (± 0.03)
DMF	calculated [b] ($mmol_{CO2}\ g_{CAT}^{-1}$)	0.62 (<± 0.01)	0.59 (± 0.01)
	ratio (%)	11.9 (± 0.3)	7.2 (± 0.2)
	predicted [f] ($mmol_{CO2}\ g_{CAT}^{-1}$)	0.11(± 0.01)	0.09 (<± 0.01)
Cl_{SUP} (or Cl^{-}_{SUP})	calculated [b] ($mmol_{CO2}\ g_{CAT}^{-1}$)	-	2.69 (± 0.03)
	ratio (%)	-	32.7 (± 1.0)
	predicted [f] ($mmol_{CO2}\ g_{CAT}^{-1}$)	-	0.42 (± 0.01)

[a] Lewis acidic site (LA) only. [b] via titration and ^{1}H-NMR of (digested) UiO-66/UiO-66-Cl. [c] via CO isotherm at 20 °C and P/P_0~ 1.0. [d] summation of Lewis acidic site (LA), Brönsted acidic site (BA), DMF, and Cl_{SUP}/Cl^{-}_{SUP}. [e] via CO_2 isotherm at 20 °C and P/P_0~ 1.0. [f] N_{CO2} multiplied by ratio.

Table S8. Coefficients used to simulate CO_2 isotherms for UiO-66 and UiO-66-Cl.

temperature (°C)	coefficient	UiO-66	UiO-66-Cl
-20	A [a, b] ($mmol_{CO2}$ g_{CAT}^{-1})	16.79	116.71
	B [a, b] (bar^{-1})	0.43	0.18
	C [a, b] (dimensionless)	0.38	0.28
0	A [a, b] ($mmol_{CO2}$ g_{CAT}^{-1})	9.94	113.34
	B [a, b] (bar^{-1})	0.23	0.07
	C [a, b] (dimensionless)	0.56	0.31
20	A [a, b] ($mmol_{CO2}$ g_{CAT}^{-1})	2.65	100.34
	B [a, b] (bar^{-1})	0.46	0.03
	C [a, b] (dimensionless)	1.00	0.31
20	$S_{BET, CO2}$ [a, c] (m_{CO2}^2 g_{CAT}^{-1})	54.9 (± 2.2)	77.4 (± 4.7)
	N_{CO2} [a, d] ($mmol_{CO2}$ g_{CAT}^{-1})	0.99 (± 0.05)	1.28 (± 0.01)
	S_{CO2} [a, e] ($X10^4$ m_{CO2}^2 mol_{CO2}^{-1})	5.5 (± 0.4)	6.0 (± 0.4)

[a] See Fig. S10. [b] via Toth fitting at $0<P/P_0\leq1.0$. [c] via BET at $0.05\leq P/P_0\leq0.30$. [d] moles of CO_2 adsorbed at P/P_0 of ~1.0. [e] $S_{BET, CO2}$ divided by N_{CO2}.

Table S9. Coefficients used to simulate CO isotherms for UiO-66 and UiO-66-Cl.

temperature (°C)	coefficient	UiO-66	UiO-66-Cl
-20	A [a, b] (μmol_{CO} g_{CAT}^{-1})	834.82	70075.86
	B [a, b] (bar^{-1})	0.27	0.01
	C [a, b] (dimensionless)	2.52	0.38
0	A [a, b] (μmol_{CO} g_{CAT}^{-1})	615.55	4541.87
	B [a, b] (bar^{-1})	0.24	0.05
	C [a, b] (dimensionless)	2.57	1.77
20	A [a, b] (μmol_{CO} g_{CAT}^{-1})	441.15	2532.67
	B [a, b] (bar^{-1})	0.17	0.03
	C [a, b] (dimensionless)	7.84	2.59
20	$S_{BET, CO}$ [a, c] (m_{CO}^2 g_{CAT}^{-1})	3.8 (± 0.3)	7.3 (± 3.3)
	N_{CO} [a, d] ($mmol_{CO}$ g_{CAT}^{-1})	0.08 (± 0.01)	0.07 (<± 0.01)
	S_{CO} [a, e] ($X10^5$ m_{CO}^2 mol_{CO}^{-1})	0.5 (± 0.2)	1.1 (± 0.5)

[a] See Fig. S11. [b] via Toth fitting at $0<P/P_0\leq1.0$. [c] via BET at $0.05\leq P/P_0\leq0.30$. [d] moles of CO adsorbed at P/P_0 of ~1.0. [e] $S_{BET, CO}$ divided by N_{CO}.

Table S10. Parameters used to simulate EPR spectra of reaction solutions and mixtures.

	DMPO-OH [a]		reference
hyperfine splitting constant	a(^{14}N)	14.80 G	32
	a(^{1}H)	14.80 G	32
peak-to-peak linewidth	0.6 G (Gaussian) or 0.5 G (Lorentzian) for UiO-66 (reaction solution) [b]		
	0.2 G (Gaussian) or 0.1 G (Lorentzian) for UiO-66-Cl (reaction solution) [b]		
	0.6 G (Gaussian) or 0.5 G (Lorentzian) for UiO-66 (reaction mixture) [b]		
	0.1 G (Gaussian) or 0.8 G (Lorentzian) for UiO-66-Cl (reaction mixture) [b]		
	0.5 G (Gaussian) or 0.1 G (Lorentzian) for UiO-66-Cl (reaction mixture) [c]		
g-factor [d]	2.006		
	DMPO-OOH [a]		
hyperfine splitting constant	a(^{14}N)	14.14 G	33
	a(^{1}H)	11.83 G	33
	a(^{1}H)	0.88 G	33
peak-to-peak linewidth	5.0 G (Gaussian) or 3.0 G (Lorentzian) for UiO-66 (reaction solution) [b]		
	1.0 G (Gaussian) or 0.5 G (Lorentzian) for UiO-66-Cl (reaction solution) [b]		
	0.5 G (Gaussian) or 2.0 G (Lorentzian) for UiO-66 (reaction mixture) [b]		
	1.0 G (Gaussian) or 0.1 G (Lorentzian) for UiO-66-Cl (reaction mixture) [b]		
	0.5 G (Gaussian) or 1.0 G (Lorentzian) for UiO-66-Cl (reaction mixture) [c]		
g-factor [d]	2.006		
	HDMPO-OH [a]		
hyperfine splitting constant	a(^{14}N)	15.30 G	34
	a(^{1}H)	1.20 G	34
peak-to-peak linewidth	0.5 G (Gaussian) or 1.0 G (Lorentzian) for UiO-66 (reaction solution) [b]		
	3.0 G (Gaussian) or 1.0 G (Lorentzian) for UiO-66-Cl (reaction solution) [b]		
	4.0 G (Gaussian) or 6.0 G (Lorentzian) for UiO-66 (reaction mixture) [b]		
	5.0 G (Gaussian) or 3.0 G (Lorentzian) for UiO-66-Cl (reaction mixture) [b]		
	1.5 G (Gaussian) or 1.0 G (Lorentzian) for UiO-66-Cl (reaction mixture) [c]		
g-factor [d]	2.006		
	DMPO-X [a]		
hyperfine splitting constant	a(^{14}N)	7.20 G	35
	a(^{1}H)	4.10 G	35
	a(^{1}H)	3.90 G	35
peak-to-peak linewidth	1.0 G (Gaussian) or 2.0 G (Lorentzian) for UiO-66-Cl (reaction solution) [b]		
	3.0 G (Gaussian) or 1.0 G (Lorentzian) for UiO-66-Cl (reaction mixture) [b]		
	2.5 G (Gaussian) or 1.5 G (Lorentzian) for UiO-66-Cl (reaction mixture) [c]		
g-factor [d]	2.006		

[a] via Gaussian and Lorentzian fitting. (See Fig. 4 and S13.) [b] pH of <2.0. [c] pH of ~8.3 (using NaOH). [d] g= 714.47 X V X B^{-1}, in which V and B refer to as resonance frequency (9.6450 GHz) and center magnetic field (3435 G), respectively.

Table S11. Relative abundance of DMPO-OH, DMPO-OOH, HDMPO-OH, or DMPO-X adducts simulated for EPR spectra of reaction solutions/mixtures.

	abundance simulated (%)			
	DMPO-OH	DMPO-OOH	HDMPO-OH	DMPO-X
UiO-66 (reaction solution) [a, b]	40.9	29.5	29.6	-
UiO-66-Cl (reaction solution) [a, b]	25.6	18.6	20.9	34.9
UiO-66 (reaction mixture) [a, c]	41.6	29.2	29.2	-
UiO-66-Cl (reaction mixture) [a, c]	23.8	19.1	21.4	35.7
UiO-66-Cl (reaction mixture) [c, d]	10.6	10.6	36.2	42.6

[a] pH of <2.0. [b] See Fig. S14. [c] See Fig. 4E-4G. [d] pH of ~8.3 (using NaOH).

Table S12. Apparent reaction rate constants (k_{APP}) of control reactions.

reactant	figure	material	k_{APP} [a] (X10^{-3} min^{-1})	regression factor (R^2) [a]
H_2O_2	Fig. S12 [d, e, f]	UiO-66	0.09 (± 0.01)	0.95
		UiO-66-Cl	0.13 (± 0.01)	0.80
phenol [b]	Fig. S16 [d, e]	UiO-66 (d_{PARTICLE}<20 µm; 300 rpm)	0.42 (± 0.05)	0.80
		UiO-66 (20≤d_{PARTICLE}<45 µm; 300 rpm)	0.38 (± 0.04)	0.88
		UiO-66 (d_{PARTICLE}<60 µm; 300 rpm)	0.36 (± 0.03)	0.87
		UiO-66 (d_{PARTICLE}<60 µm; 400 rpm)	0.41 (± 0.04)	0.85
		UiO-66-Cl (d_{PARTICLE}<20 µm; 300 rpm)	0.72 (± 0.07)	0.80
		UiO-66-Cl (20≤d_{PARTICLE}<45 µm; 300 rpm)	0.71 (± 0.05)	0.90
		UiO-66-Cl (d_{PARTICLE}<60 µm; 300 rpm)	0.76 (± 0.06)	0.92
		UiO-66-Cl (d_{PARTICLE}<60 µm; 400 rpm)	0.77 (± 0.07)	0.89
	Fig. S19A [d, e, f, g]	UiO-66 (without scavenger) [i]	0.36 (± 0.03)	0.87
		UiO-66 (with acetone)	0.28 (± 0.02)	0.89
		UiO-66 (with 1,4-dioxane)	0.22 (± 0.02)	0.92
		UiO-66 (with catechol)	0.18 (± 0.02)	0.80
	Fig. S19B [d, e, f, h]	UiO-66-Cl (without scavenger) [i]	0.76 (± 0.06)	0.92
		UiO-66-Cl (with acetone)	0.37 (± 0.03)	0.91
		UiO-66-Cl (with 1,4-dioxane)	0.43 (± 0.04)	0.90
		UiO-66-Cl (with catechol)	0.26 (± 0.02)	0.91
nitrobenzene [b]	Fig. S20 [d, e, f]	UiO-66	0.31 (± 0.05)	0.94
		UiO-66-Cl	0.02 (<± 0.01)	0.85
phenol [b]		UiO-66 [i]	0.36 (± 0.03)	0.87
		UiO-66-Cl [i]	0.76 (± 0.06)	0.92
aniline [b]		UiO-66	0.49 (± 0.04)	0.89
		UiO-66-Cl	1.25 (± 0.16)	0.83
phenol [b]	Fig. S21 [d, f]	UiO-66 (at 25 °C) [i]	0.36 (± 0.03)	0.87
		UiO-66 (at 35 °C)	0.54 (± 0.05)	0.87
		UiO-66 (at 45 °C)	0.81 (± 0.17)	0.85
		UiO-66 (at 55 °C)	1.41 (± 0.07)	0.97
		UiO-66-Cl (at 25 °C) [i]	0.76 (± 0.06)	0.92
		UiO-66-Cl (at 35 °C)	1.24 (± 0.09)	0.90
		UiO-66-Cl (at 45 °C)	1.66 (± 0.14)	0.86
		UiO-66-Cl (at 55 °C)	2.11 (± 0.17)	0.87
	Fig. S22 [d, e, f]	UiO-66 (1st cycle) [i]	0.36 (± 0.03)	0.87
		UiO-66 (2nd cycle)	0.26 (± 0.02)	0.89
		UiO-66 (3rd cycle)	0.12 (± 0.01)	0.88
		UiO-66-Cl (1st cycle) [i]	0.76 (± 0.06)	0.92
		UiO-66-Cl (2nd cycle)	0.56 (± 0.04)	0.94
		UiO-66-Cl (3rd cycle)	0.44 (± 0.04)	0.87
	Fig. S26 [d, e, f]	UiO-66 [i, j]	0.36 (± 0.03)	0.87
		UiO-66-Cl [i, j]	0.76 (± 0.06)	0.92
		Mn oxide-N [j]	2.46 (± 0.09)	0.99
		Fe oxide-S [j]	1.41 (± 0.10)	0.98
acetaminophen [c]	Fig. S27 [d, e, f]	UiO-66	0.78 (± 0.09)	0.94
		UiO-66-Cl	1.86 (± 0.15)	0.97
aniline [c]		UiO-66	0.79 (± 0.10)	0.93
		UiO-66-Cl	1.72 (± 0.21)	0.93
sulfanilamide [c]		UiO-66	0.44 (± 0.06)	0.92
		UiO-66-Cl	1.09 (± 0.15)	0.92
sulfamethoxazole (SMX) [c]		UiO-66	0.44 (± 0.05)	0.93
		UiO-66-Cl	0.79 (± 0.11)	0.91

[a] via fitting of -ln ($C_{XXX}/C_{XXX,\ 0}$) versus time, in which XXX denotes phenol, nitrobenzene, aniline, acetaminophen, sulfanilamide, sulfamethoxazole (SMX), or H_2O_2. [b] 0.1 mmol of phenol, nitrobenzene, or aniline. [c] 0.007 mmol of acetaminophen, aniline, sulfanilamide, or sulfamethoxazole (SMX). [d] with the use of 30 mmol H_2O_2. [e] at 25 °C. [f] <60 µm and 300 rpm. [g] with the use of 60 mmol of scavenger. [h] with the use of 60.5 mmol of scavenger. [i] re-plotted for comparison. [j] amount of CO chemisorbed in a per-gram basis ($\mu mol_{CO}\ g_{CAT}^{-1}$ via CO-pulsed chemisorption) of 0.30 (± 0.12) for UiO-66; 0.26 (± 0.01) for UiO-66-Cl; 0.40 (± 0.02) for Mn oxide-N; 1.59 (± 0.03) for Fe oxide-S.

Table S13. Quantities of Zr/Cl, Mn/N, and Fe/S leached from UiO-66/UiO-66-Cl, Mn oxide-N, and Fe oxide-S, respectively, during phenol degradation runs.

	cycle	UiO-66	UiO-66-Cl	Mn oxide-N	Fe oxide-S
Zr leached [a] (mol. %)	1st cycle	4.5 X 10^{-6}	3.1 X 10^{-6}	-	-
	2nd cycle	1.3 X 10^{-6}	1.4 X 10^{-6}	-	-
	3rd cycle	1.3 X 10^{-6}	1.4 X 10^{-6}	-	-
Cl leached [b] (mol. %)	1st cycle	-	8.8 X 10^{-1}	-	-
	2nd cycle	-	8.8 X 10^{-1}	-	-
	3rd cycle	-	1.5 X 10^{-1}	-	-
Mn leached [a] (mol. %)	1st cycle	-	-	1.9	-
N leached [c] (mol. %)		-	-	1.4	-
Fe leached [a] (mol. %)	1st cycle	-	-	-	0.1
S leached [a] (mol. %)		-	-	-	3.0

[a] via ICP. [b] via IC. [c] via TN.

Table S14. Lengths of four Zr-O_A bonds ($d_{Zr\text{-}OA}$; A= 1-4) present in the MOFs simplified for DFT calculations.

	UiO-66	UiO-66-Cl		
	R= H [a]	R= Cl_{SUP} [a]	R= Cl^{-}_{SUP} [a]	R= $Cl^{\bullet}_{SUP}$ [a]
$d_{Zr\text{-}O1}$ (Å)	2.12	2.08	2.12	2.15
$d_{Zr\text{-}O2}$ (Å)	2.83	2.14	3.01	3.17
$d_{Zr\text{-}O3}$ (Å)	2.14	2.12	2.07	2.08
$d_{Zr\text{-}O4}$ (Å)	3.23	2.18	2.80	2.82
average (Å)	2.58	2.13	2.50	2.56

[a] See Fig. S23.

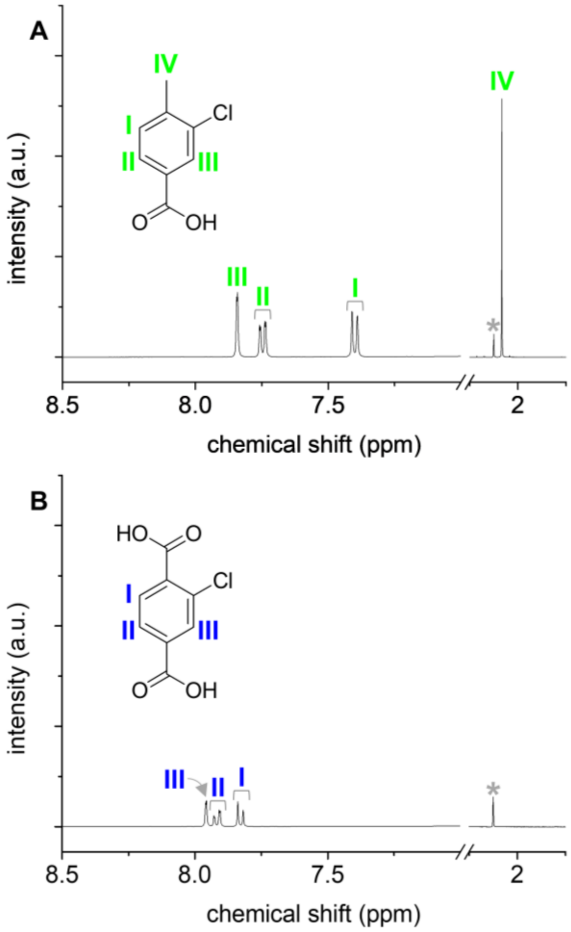

Fig. S1. ^{1}H-NMR spectra of 3-chloro-4-methylbenzoic acid (A) and 2-chlorobenzene-1,4-dicarboxylic acid (B) dissolved in aqueous HF. In (A-B), peaks marked with * denote dimethyl sulfoxide (DMSO)-d_6 (NMR solvent).

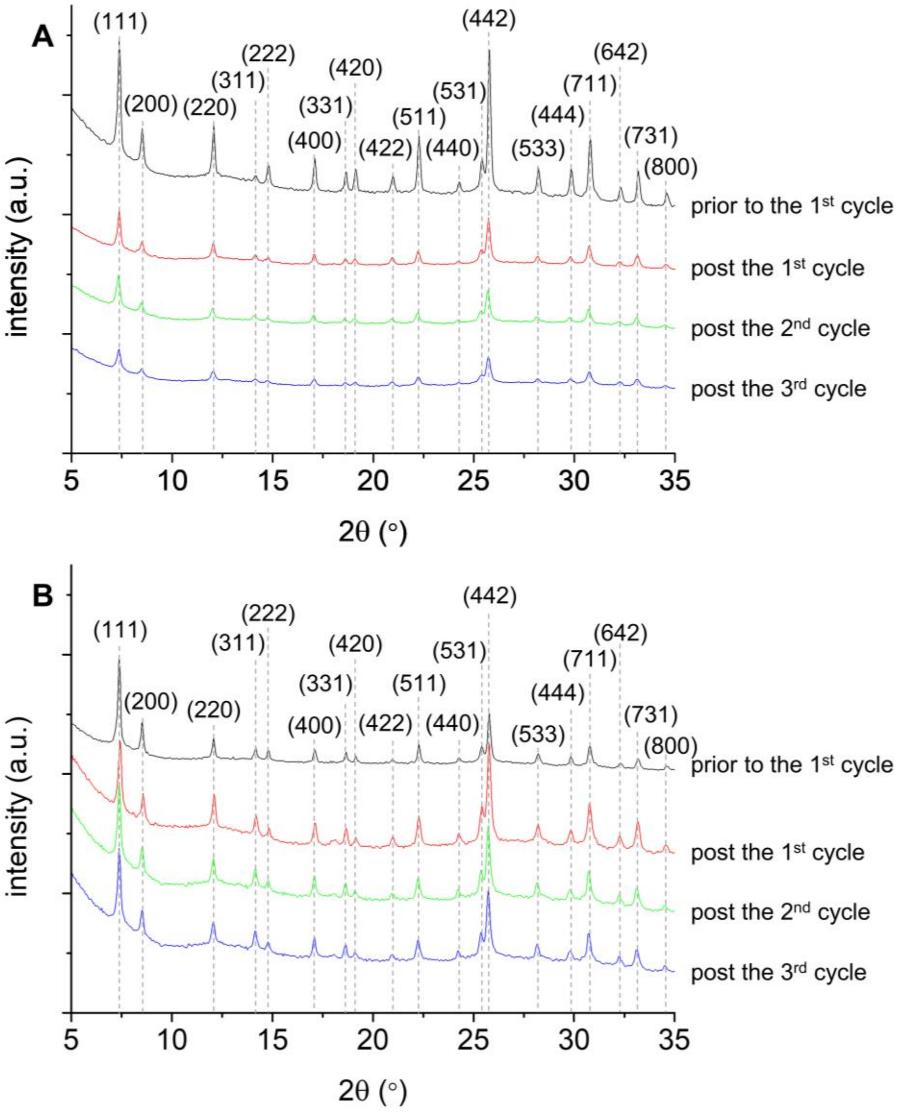

Fig. S2. XRD patterns of UiO-66 (A) and UiO-66-Cl (B) post being subjected to SC-CO_2 extraction (prior to the 1st cycle) and phenol degradation recycle runs (post the 1st, 2nd, and 3rd cycles). In (A-B), diffractions marked with (*hkl*) are indexed to those of *face-centered cubic* UiO-66 simulated (CCDC No. of 1018045).

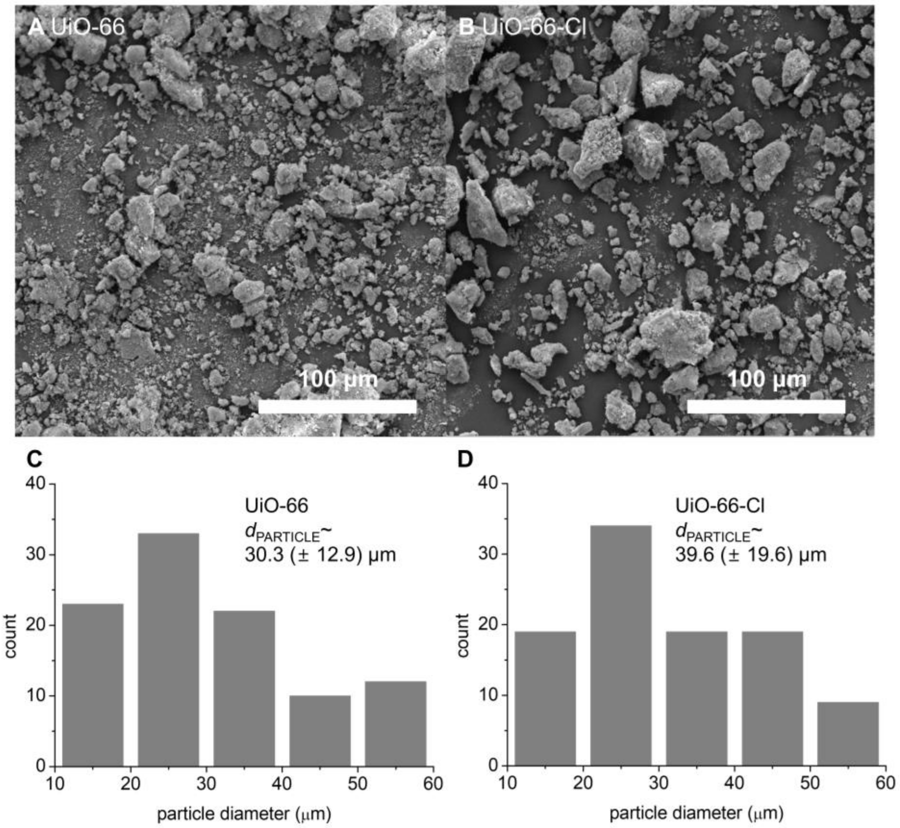

Fig. S3. SEM images of UiO-66 (A) and UiO-66-Cl (B) and their particle size distributions (UiO-66 for (C); UiO-66-Cl for (D); number of particles counted~ 100). In (C-D), d_{PARTICLE} indicates particle diameter of UiO-66 or UiO-66-Cl.

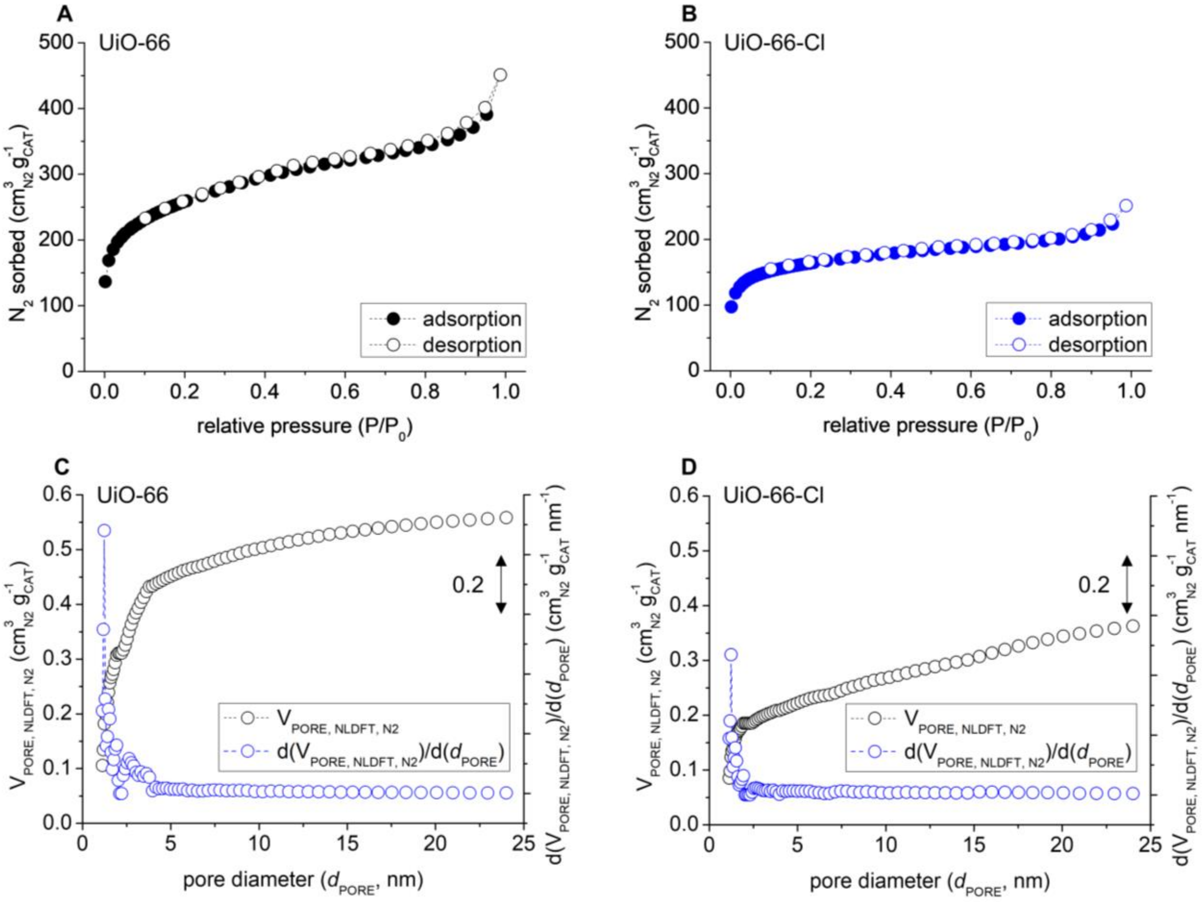

Fig. S4. N_2 isotherms of UiO-66 (A) and UiO-66-Cl (B) and their pore size (d_{PORE}) distributions assessed via NLDFT technique (UiO-66 for (C); UiO-66-Cl for (D)).

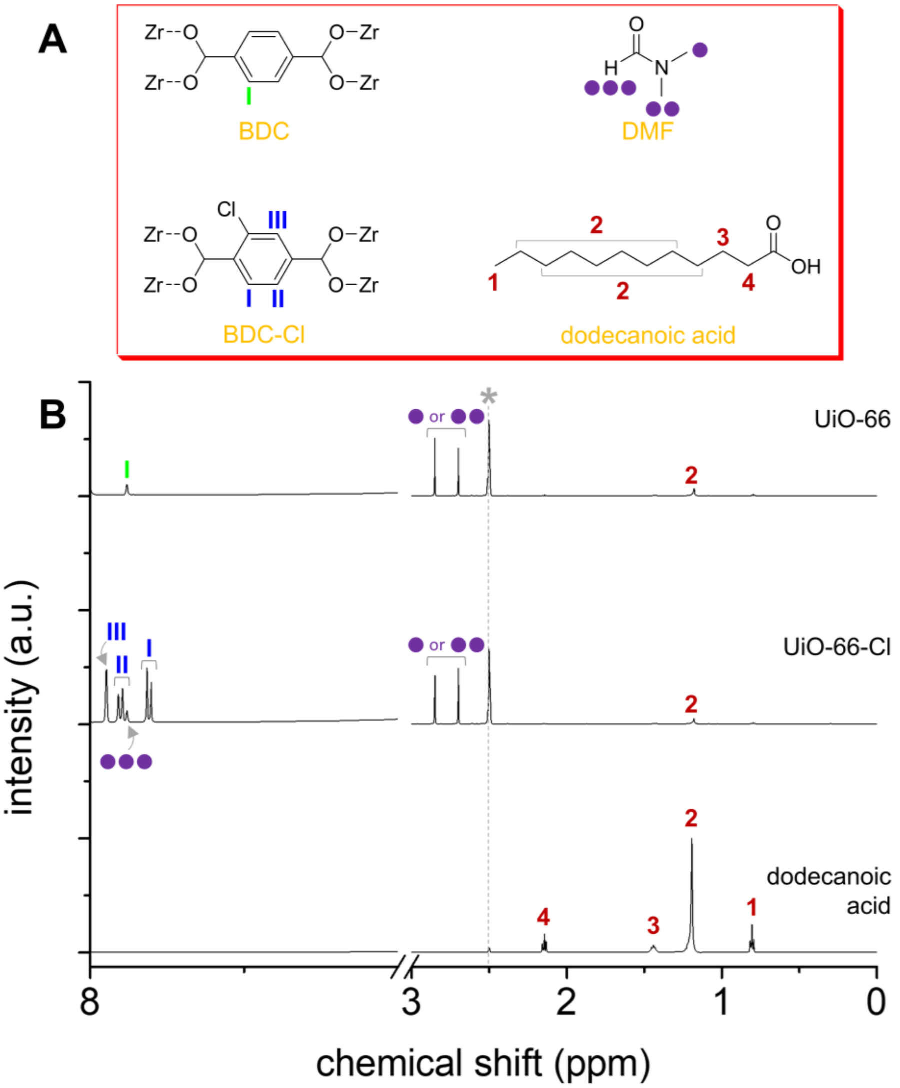

Fig. S5. (A) Illustration of benzene-1,4-dicarboxylate (BDC), 2-chlorobenzene-1,4-dicarboxylate (BDC-Cl), and N,N'-dimethyl formamide (DMF) used to build UiO-66/UiO-66-Cl architectures alongside with their structural modulator (dodecanoic acid). (B) ^{1}H-NMR spectra of UiO-66, UiO-66-Cl, and dodecanoic acid dissolved in aqueous HF. In (B), peaks marked with * denote DMSO-d_6 (NMR solvent), whereas peaks marked with I (green for BDC), III (blue for BDC-Cl), and ●/●● (purple for DMF) served to quantify DMF relative to BDC (or BDC-Cl) via integration (Table S2) in order to determine the base unit of UiO-66 (or UiO-66-Cl). In (B), peaks marked with 2 originated from dodecanoic acid, were minute in comparison with I (green; BDC:dodecanoic acid~ 1:0.02) and III (blue; BDC-Cl:dodecanoic acid~ 1:0.01) in the molar basis (Table S2), and therefore were not considered for the determination of the base units for UiO-66 and UiO-66-Cl.

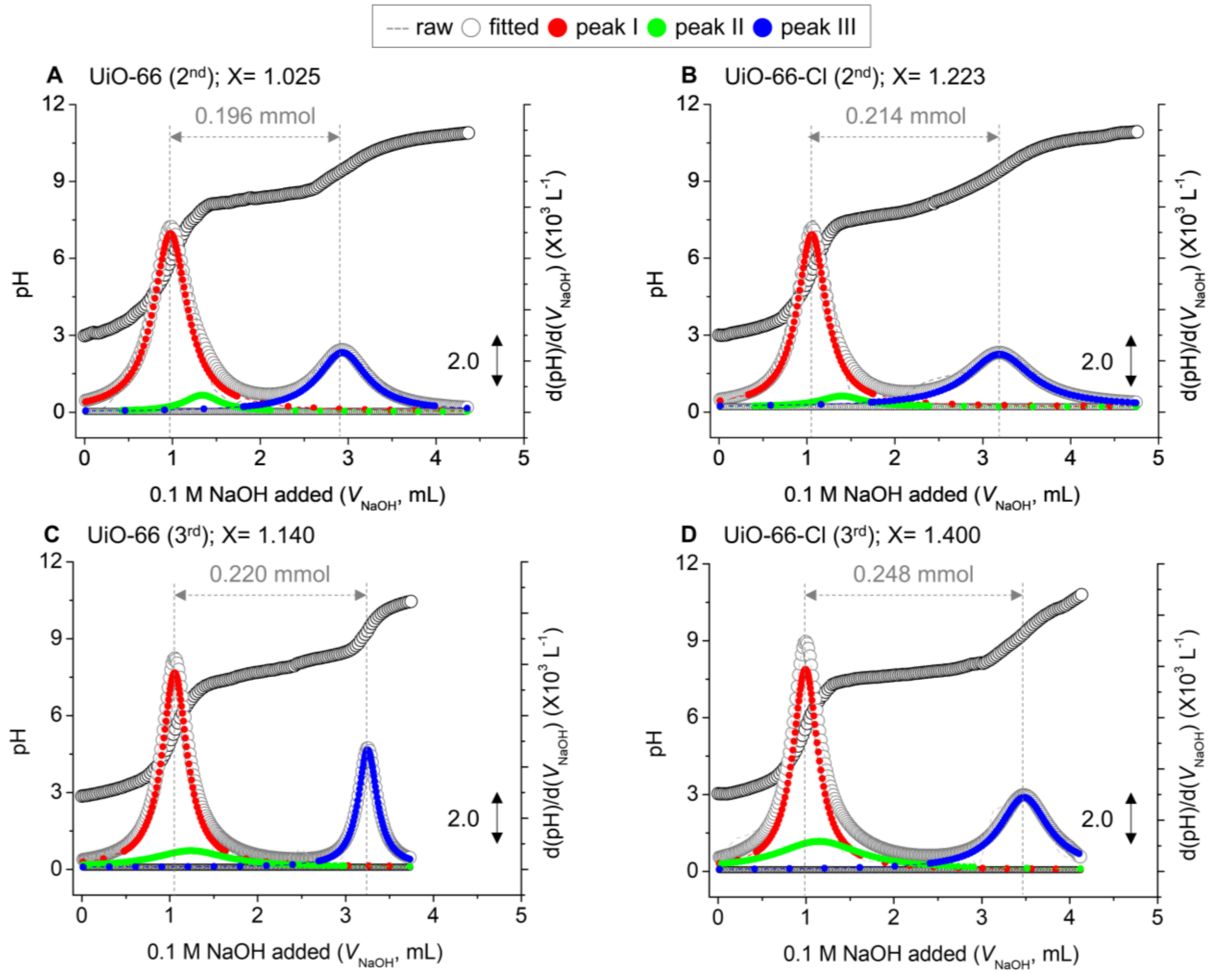

Fig. S6. Titration curves of UiO-66 (the 2nd trial for (A); the 3rd trial for (C)) and UiO-66-Cl (the 2nd trial for (B); the 3rd trial for (D)), for which HCl was initially implemented to adjust pH values of UiO-66/UiO-66-Cl dispersed in de-ionized H_2O to 3.0 for ensuring the protonation of the sites including μ_3-OH, Zr^{4+}-H_2O, and Zr^{4+}-OH, whereas NaOH served as a titrant. Protons could then be desorbed from the sites upon the increase in pH values in the sequence of μ_3-OH$\rightarrow$$Zr^{4+}$-$H_2O$$\rightarrow$-OH on Zr^{4+}-OH, by which the resulting protons liberated could equilibrate with OH^- of NaOH fed at equivalent points (peak I/II/III), as listed in Table S3. In (A-D), black empty circle denotes the plot of pH value versus the volume of 0.1 M NaOH added (V_{NaOH}) for UiO-66 (or UiO-66-Cl). In addition, X denotes the number of missing organic struts (BDC or BDC-Cl) for the base unit of UiO-66 (or UiO-66-Cl), whereas the difference in V_{NaOH} values for peak I and peak III was utilized to calculate the quantity of missing organic struts in a per-gram of UiO-66 (or UiO-66-Cl).

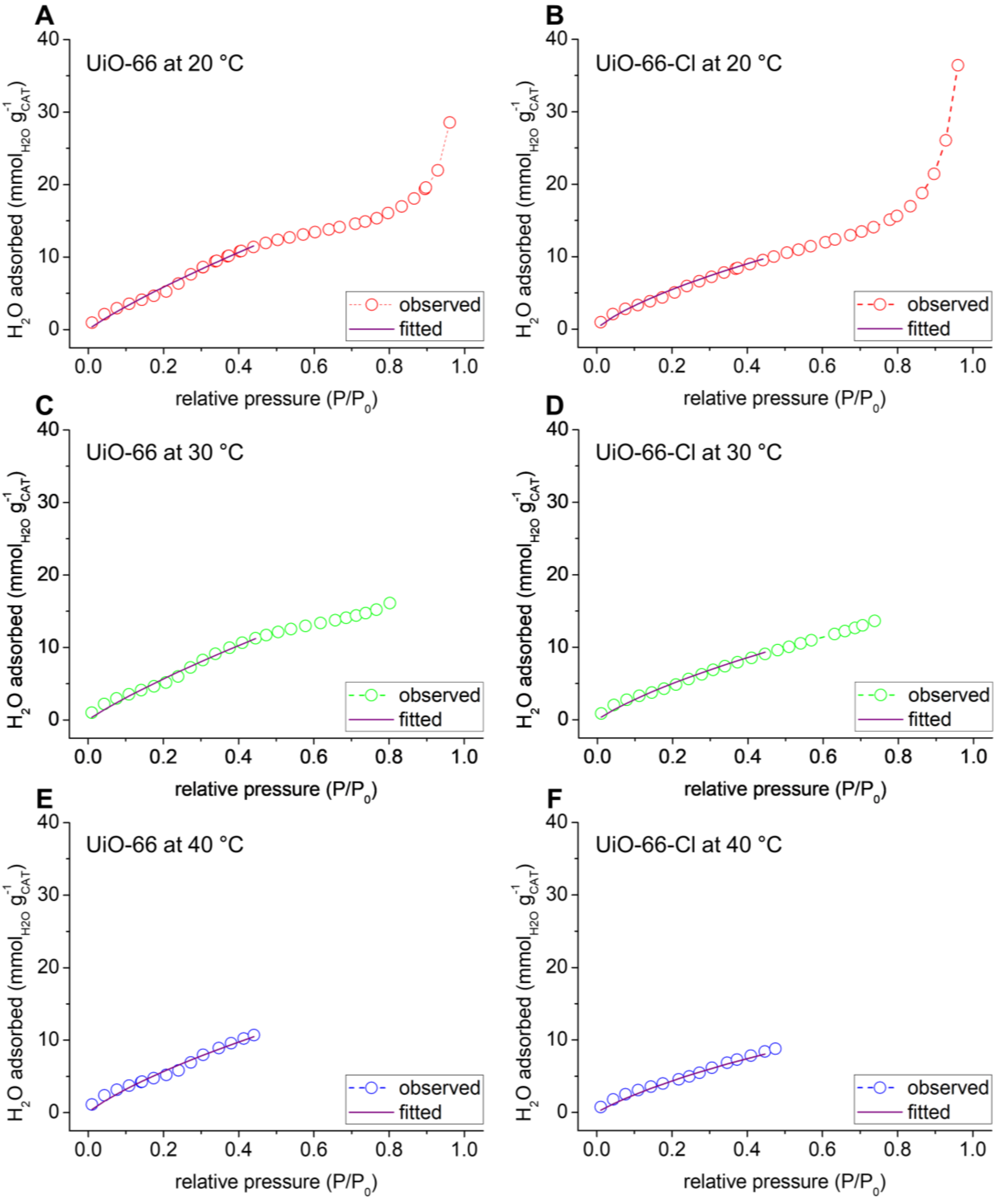

Fig. S7. H_2O adsorption isotherms of UiO-66 and UiO-66-Cl collected at 20-40 °C (20 °C for (A-B); 30 °C for (C-D); 40 °C for (E-F)), where P/P_0 ranges are 0-1.0 for 20 °C, 0-0.80 for 30 °C, and 0-0.44 for 40 °C due to the instrumental limitation. H_2O adsorption isotherms were thus fitted using Toth equation with P/P_0 range of 0-0.44 and shown with purple solid lines. (Details can be found in Table S5.)

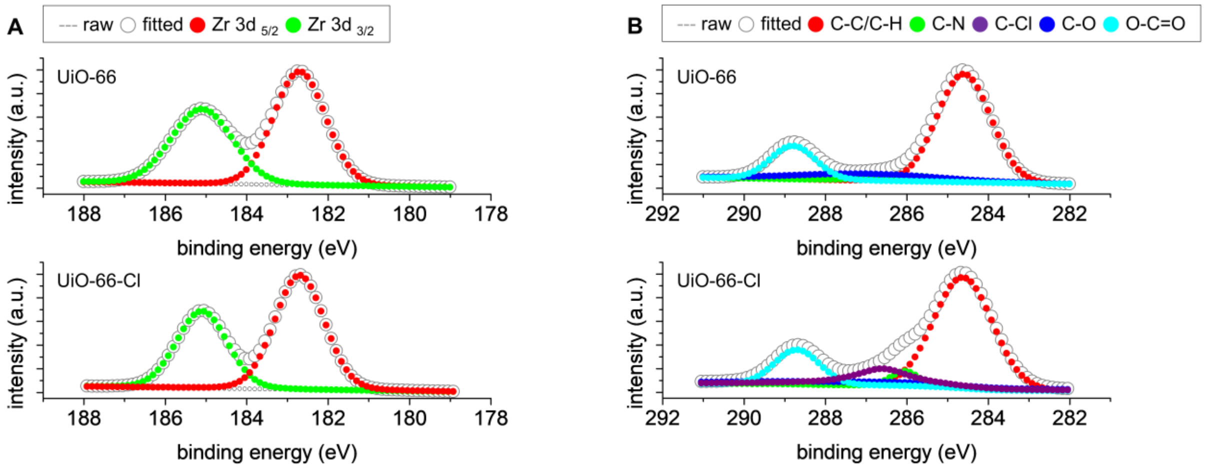

Fig. S8. XP spectra of UiO-66 and UiO-66-Cl in the Zr 3d (A) and C 1s domains (B). In (A-B), gray dashed lines, gray empty circles, and black empty circles denote raw XP spectra, fitted XP spectra, and backgrounds, respectively. Locations of surface phases and their concentrations are tabulated in Table S6.

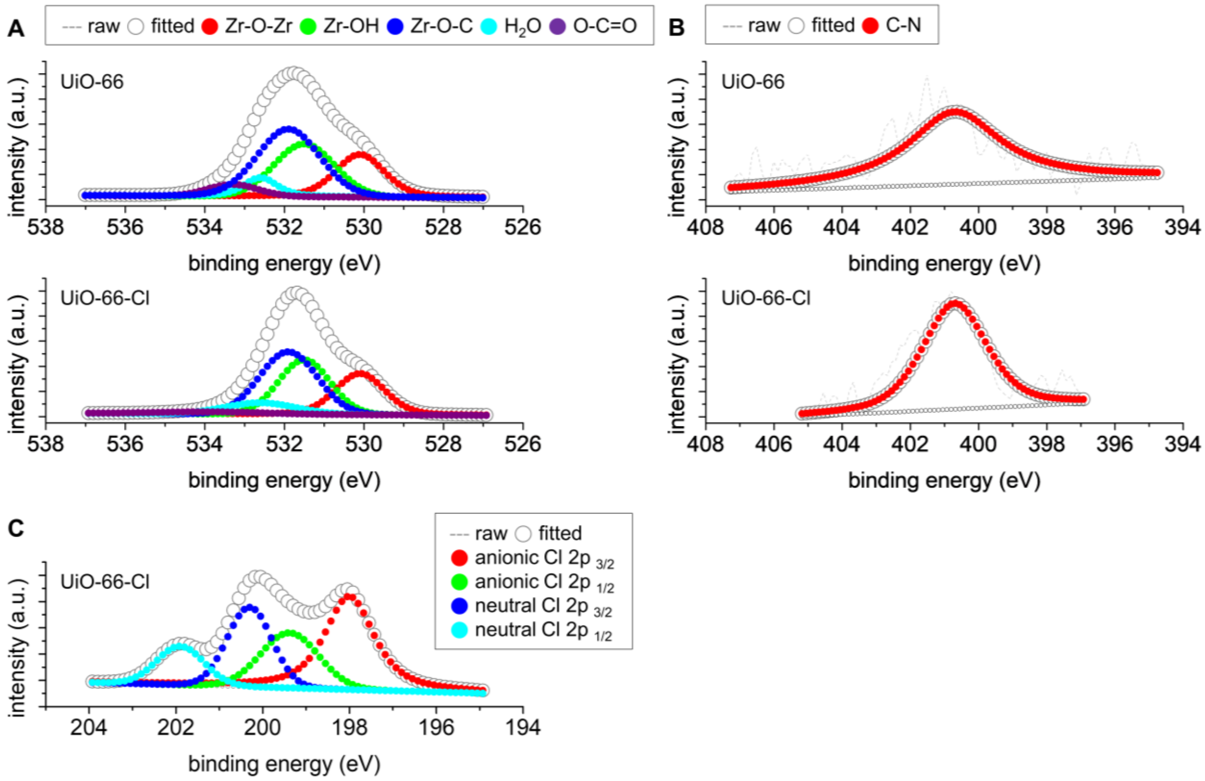

Fig. S9. XP spectra of UiO-66 and UiO-66-Cl in the O 1s (A), N 1s (B), and Cl 2p domains (C). In (A-C), gray dashed lines, gray empty circles, and black empty circles denote raw XP spectra, fitted XP spectra, and backgrounds, respectively. Locations of surface phases and their concentrations are tabulated in Table S6.

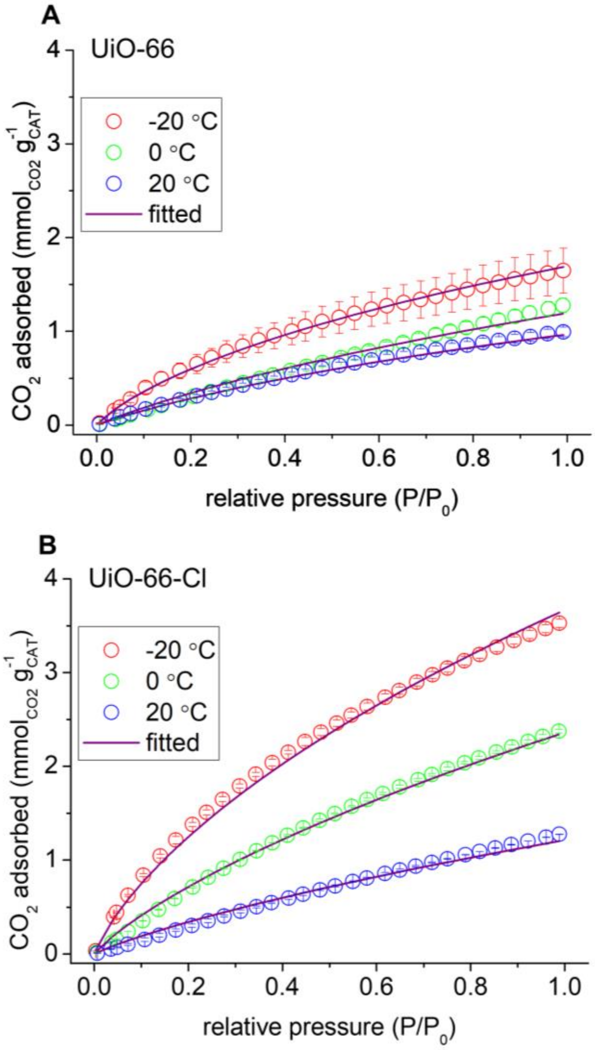

Fig. S10. CO_2 adsorption isotherms of UiO-66 (A) and UiO-66-Cl (B) collected at -20-20 °C with P/P_0 range of 0-1.0. In (A-B), CO_2 adsorption isotherms were fitted using Toth equation and shown with purple solid lines. (Details can be found in Table S8.)

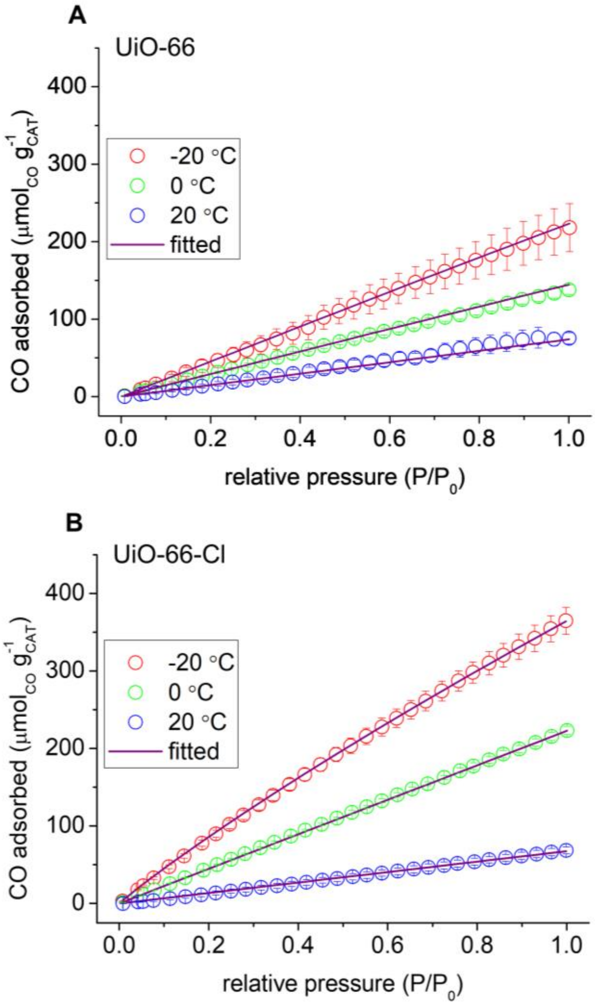

Fig. S11. CO adsorption isotherms of UiO-66 (A) and UiO-66-Cl (B) collected at -20-20 °C with P/P_0 range of 0-1.0. In (A-B), CO adsorption isotherms were fitted using Toth equation and shown with purple solid lines. (Details can be found in Table S9.)

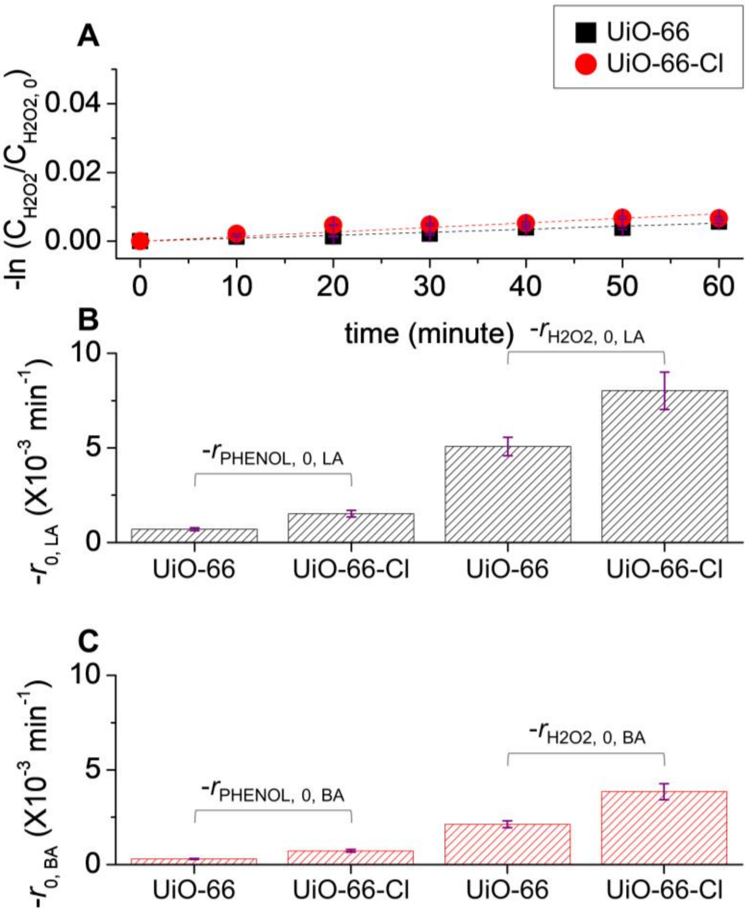

Fig. S12. (A) Fittings of background-subtracted reaction data to pseudo-1st-order kinetic model (-ln ($C_{H2O2}/C_{H2O2,\,0}$) versus time) to assess apparent reaction rate constants (k_{APP} values in Table S12) of UiO-66/UiO-66-Cl in dissecting H_2O_2. In (A), background denotes H_2O_2 self-dissection (in the absence of UiO-66/UiO-66-Cl) under the reaction environments specified below. $C_{H2O2,\,0}$ and C_{H2O2} indicate H_2O_2 concentration initially fed and H_2O_2 concentration present in reaction mixture at a specific reaction time, respectively. Background-subtracted initial H_2O_2 dissection rates ($-r_{H2O2,\,0}$) and background-subtracted initial phenol degradation rates ($-r_{PHENOL,\,0}$ from the plots of 'without scavenger' in Fig. S19) of UiO-66/UiO-66-Cl in a per-Lewis acidic (LA) site or in a per-Brönsted acidic (BA) site basis: $-r_{PHENOL,\,0,\,LA}$ and $-r_{H2O2,\,0,\,LA}$ for (B) and $-r_{PHENOL,\,0,\,BA}$ and $-r_{H2O2,\,0,\,BA}$ for (C). Reaction conditions: 0.2 g of UiO-66 (or UiO-66-Cl) with sizes of <60 µm; 30 mmol of H_2O_2; 100 mL of de-ionized H_2O; initial pH of 7.0; 25 °C; 300 rpm.

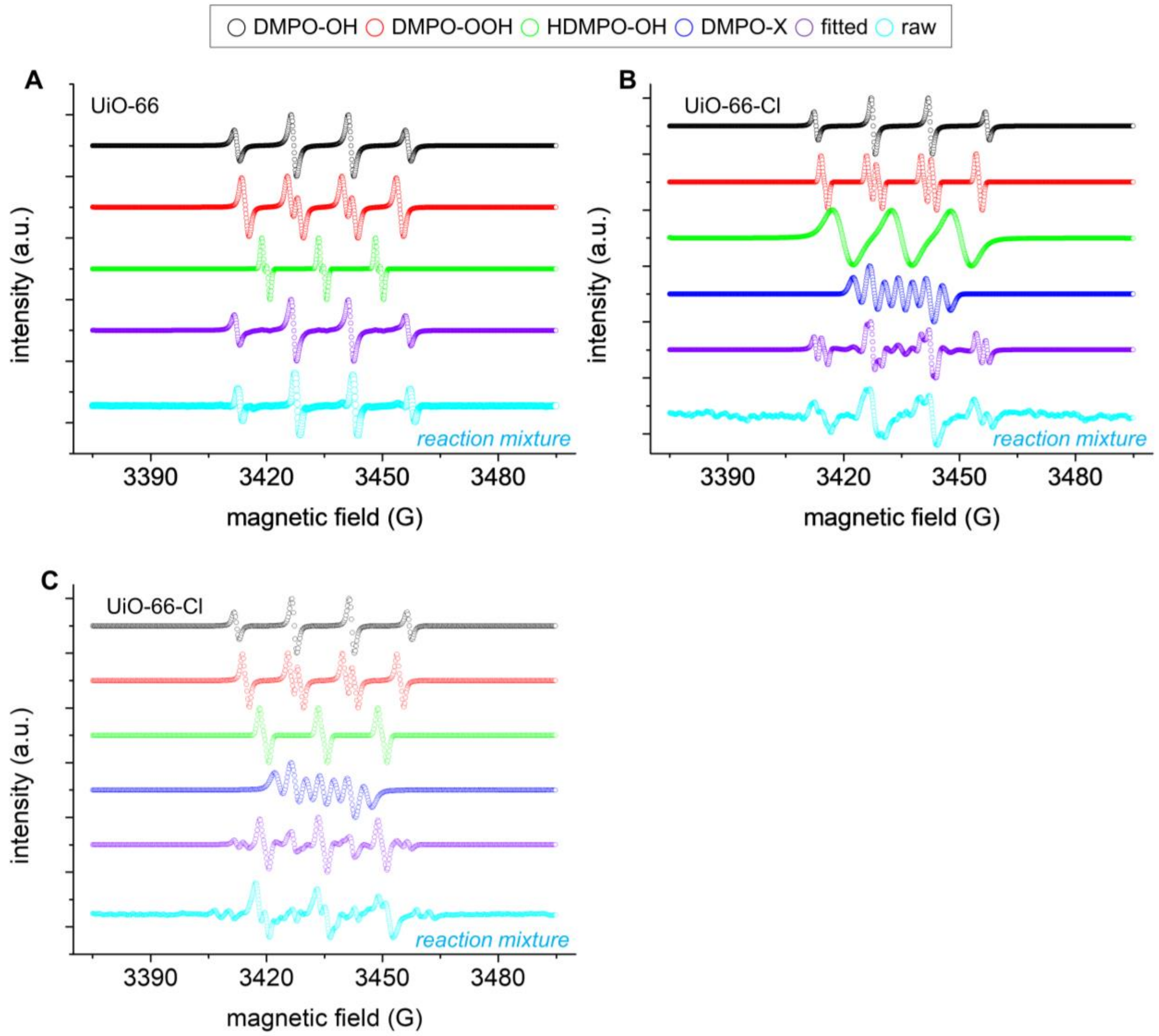

Fig. S13. EPR spectra of reaction mixtures containing H_2O_2, DMPO, and UiO-66 (A)/UiO-66-Cl (B-C) under acidic (A-B; pH of <2.0) or basic pH environment (C; pH of ~8.3). In (A-C), black, red, green, and blue empty circles indicate individual EPR spectra simulated for DMPO-OH, DMPO-OOH, HDMPO-OH, and DMPO-X adducts, respectively. In addition, purple and cyan empty circles correspond to convoluted and raw EPR spectra, respectively. Analytic conditions: 0.2 g of de-ionized H_2O; 3.0 mmol of H_2O_2; 0.7 mmol of DMPO; 0.1 g of UiO-66 (or UiO-66-Cl); stirred using vortex for 2 minutes.

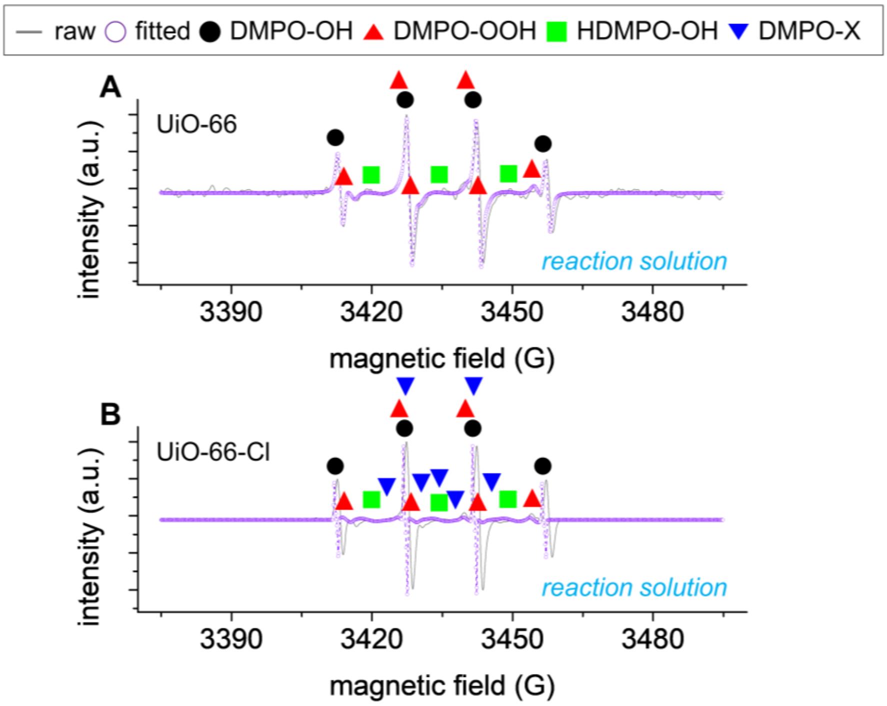

Fig. S14. EPR spectra of reaction solutions collected via filtration of reaction mixtures containing H_2O_2, 5,5-dimethyl-1-pyrroline N-oxide (DMPO; spin trapper), UiO-66 (A), or UiO-66-Cl (B). In (A-B), gray solid lines and violet empty circles indicate raw and simulated EPR spectra, respectively. (See parameters utilized to simulate EPR spectra in Table S10.) Black solid circles, red solid upper triangle, green solid square, and blue solid lower triangle refer to as DMPO-OH, DMPO-OOH, HDMPO-OH, and DMPO-X adducts, respectively, whose relative abundance is listed in Table S11. Analytic conditions: 0.2 g of de-ionized H_2O; 3.0 mmol of H_2O_2; 0.7 mmol of DMPO; 0.1 g of UiO-66 (or UiO-66-Cl); stirred using vortex for 2 minutes.

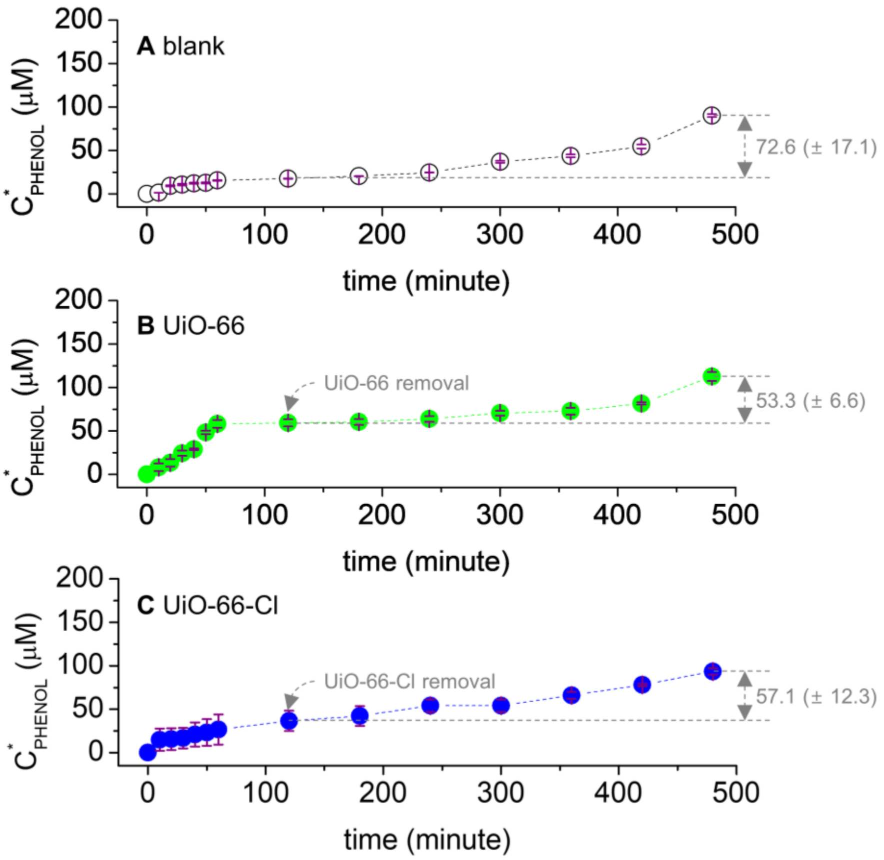

Fig. S15. Molar concentration of phenol consumed (C^*_{PHENOL}) versus time in the absence (blank for (A)) or presence of UiO-66 (B)/UiO-66-Cl (C), for which UiO-66 (or UiO-66-Cl) was vacuum-filtered after 120 minutes of reaction run for monitoring C^*_{PHENOL} values of the resulting filtrate up to 480 minutes of reaction run. Reaction conditions: 0 or 0.2 g of UiO-66 (or UiO-66-Cl) with sizes of <60 µm; 30 mmol of H_2O_2; 0.1 mmol of phenol; 100 mL of de-ionized H_2O; initial pH of 7.0; 25 °C; 300 rpm.

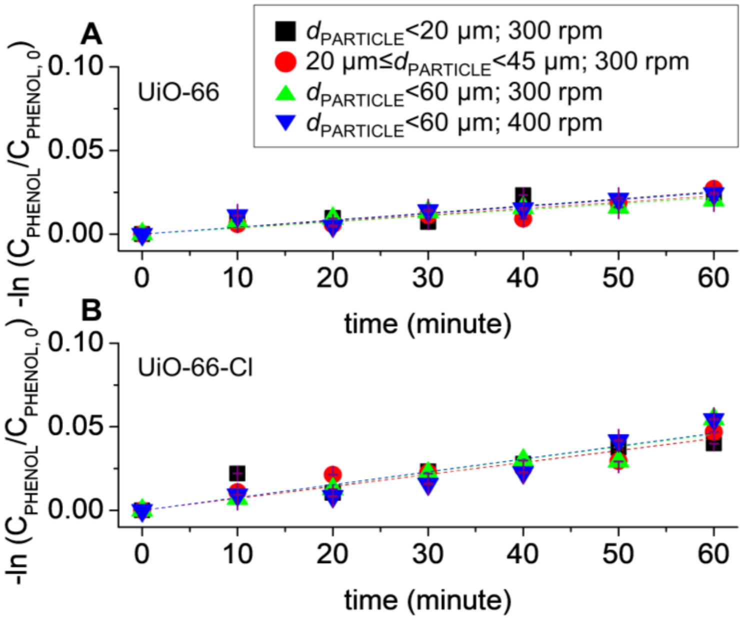

Fig. S16. Fittings of background-subtracted reaction data to pseudo-1st-order kinetic model (-ln ($C_{PHENOL}/C_{PHENOL,\ 0}$) versus time) for assessing apparent reaction rate constants (k_{APP} values in Table S12) of UiO-66 (A)/UiO-66-Cl (B) in degrading phenol with the variation of their particle diameters ($d_{PARTICLE}$; size) or stirring speeds. Background denotes phenol degradation mediated by H_2O_2 self-dissection (in the absence of UiO-66/UiO-66-Cl) or phenol adsorption on UiO-66 or UiO-66-Cl surface (in the absence of H_2O_2) under the reaction environments specified below. $C_{PHENOL,\ 0}$ and C_{PHENOL} indicate phenol concentration initially fed and phenol concentration present in reaction mixture at a specific reaction time, respectively. Reaction conditions: 0.2 g of UiO-66 (or UiO-66-Cl) with sizes of <20 µm, 20-45 µm, or <60 µm; 30 mmol of H_2O_2; 0.1 mmol of phenol; 100 mL of de-ionized H_2O; initial pH of 7.0; 25 °C; 300 rpm or 400 rpm.

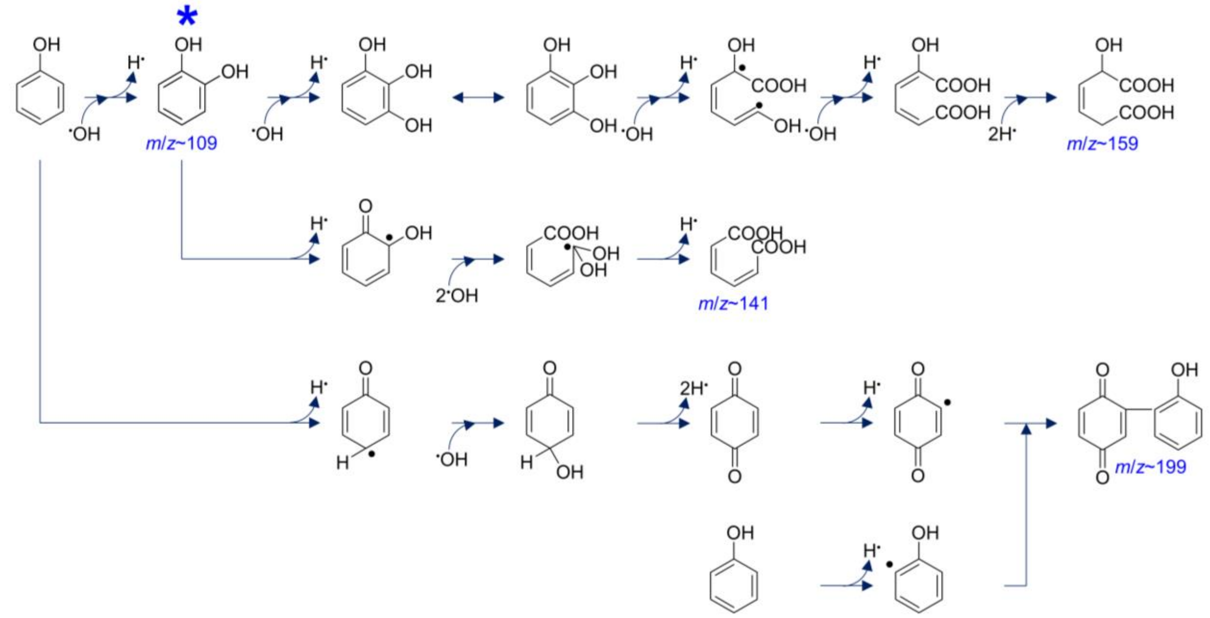

Fig. S17. Representation of phenol degradation pathways on UiO-66, where the intermediates shown with *m*/*z* values were identified using LC-MS technique in negative mode, whereas *m* and *z* indicate mass and charge, respectively. * is referred to as catechol evolved via •OH addition to phenol followed by H• abstraction from the resulting intermediate. LC-MS spectrum of UiO-66 was recorded after an hour of its phenol degradation run under the environments specified below. Reaction conditions: 0.2 g of UiO-66 with sizes of <60 µm; 30 mmol of H_2O_2; 100 mL of de-ionized H_2O; initial pH of 7.0; 25 °C; 300 rpm.

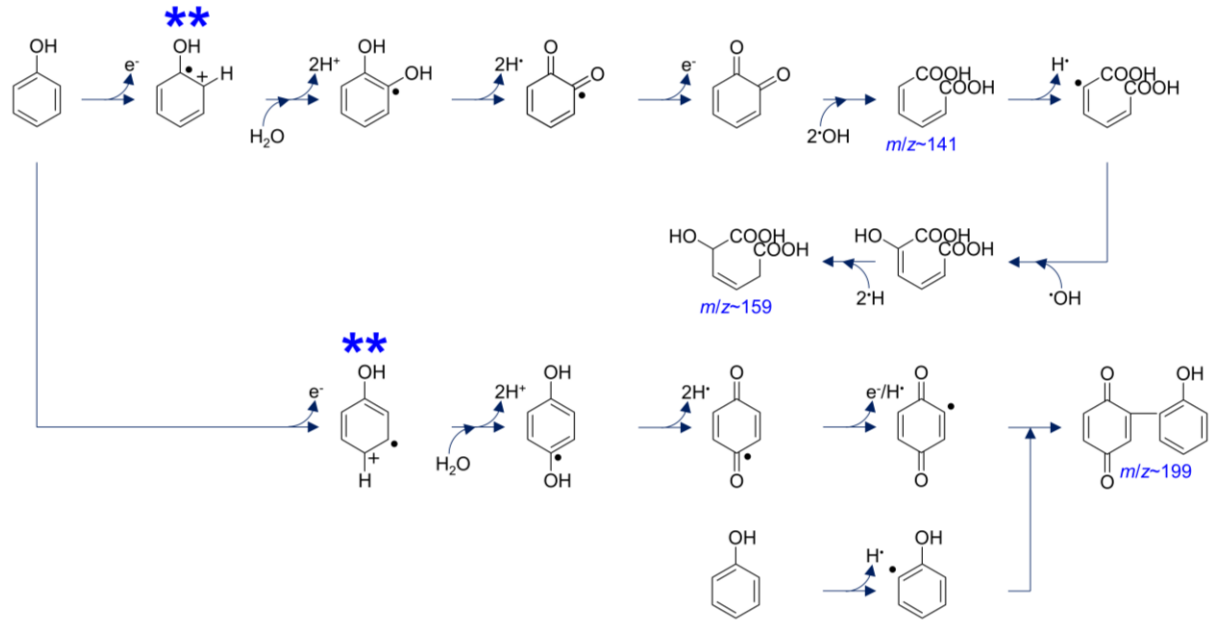

Fig. S18. Representation of phenol degradation pathways on UiO-66-Cl, where the intermediates shown with *m*/*z* values were identified using LC-MS technique in negative mode, whereas *m* and *z* indicate mass and charge, respectively. ** denotes the intermediate evolved via e^- transfer from phenol. LC-MS spectrum of UiO-66-Cl was recorded after an hour of its phenol degradation run under the environments specified below. Reaction conditions: 0.2 g of UiO-66-Cl with sizes of <60 µm; 30 mmol of H_2O_2; 100 mL of de-ionized H_2O; initial pH of 7.0; 25 °C; 300 rpm.

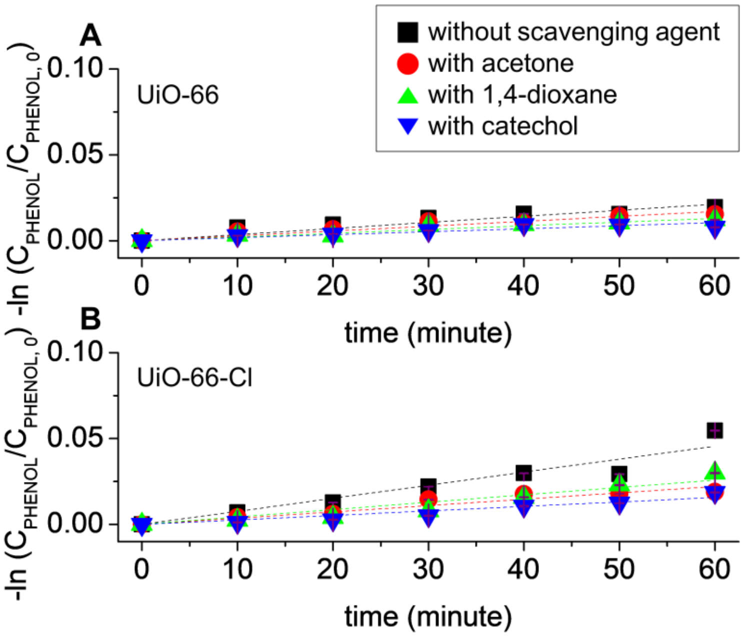

Fig. S19. Fittings of background-subtracted reaction data to pseudo-1st-order kinetic model (-ln ($C_{PHENOL}/C_{PHENOL,\ 0}$) versus time) for assessing apparent reaction rate constants (k_{APP} values in Table S12) of UiO-66 (A)/UiO-66-Cl (B) in degrading phenol in the absence or presence of scavenger (acetone, 1.4-dioxane, or catechol). In (A-B), background denotes phenol degradation mediated by H_2O_2 self-dissection (in the absence of UiO-66/UiO-66-Cl) or phenol adsorption on UiO-66 or UiO-66-Cl surface (in the absence of H_2O_2) under the reaction environments specified below. $C_{PHENOL,\ 0}$ and C_{PHENOL} indicate phenol concentration initially fed and phenol concentration present in reaction mixture at a specific reaction time, respectively. Plots of 'without scavenger' in Fig. S19 correspond to those of '$d_{PARTICLE}$<60 µm; 300 rpm' in Fig. S16 and were re-plotted for comparison. Reaction conditions: 0.2 g of UiO-66 (or UiO-66-Cl) with sizes of <60 µm; 30 mmol of H_2O_2; 0.1 mmol of phenol; 100 mL of de-ionized H_2O; scavenger of 60.0 mmol for UiO-66 or 60.5 mmol for UiO-66-Cl; initial pH of 7.0; 25 °C; 300 rpm.

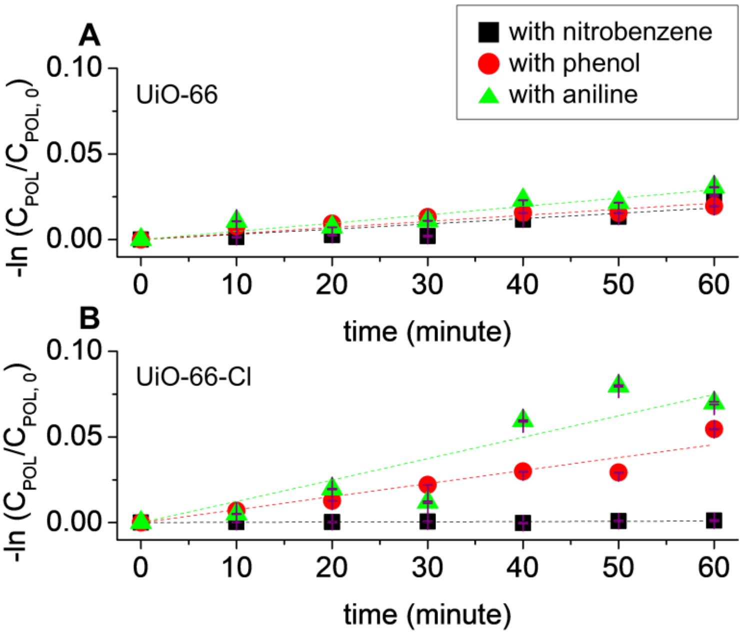

Fig. S20. Fittings of background-subtracted reaction data to pseudo-1st-order kinetic model (-ln ($C_{POL}/C_{POL,\,0}$) versus time) to assess apparent reaction rate constants (k_{APP} values in Table S12) of UiO-66 (A)/UiO-66-Cl (B) in degrading aqueous pollutant (nitrobenzene, phenol, or aniline). In (A-B), background denotes pollutant degradation mediated by H_2O_2 self-dissection (in the absence of UiO-66/UiO-66-Cl) or pollutant adsorption on UiO-66 or UiO-66-Cl surface (in the absence of H_2O_2) under the reaction environments specified below. $C_{POL,\,0}$ and C_{POL} indicate pollutant concentration initially fed and pollutant concentration present in reaction mixture at a specific reaction time, respectively. Plots of 'with phenol' ('without scavenger' in Fig. S19) were re-plotted for comparison. Reaction conditions: 0.2 g of UiO-66 (or UiO-66-Cl) with sizes of <60 µm; 30 mmol of H_2O_2; 0.1 mmol of nitrobenzene, phenol, or aniline; 100 mL of de-ionized H_2O; initial pH of 7.0; 25 °C; 300 rpm.

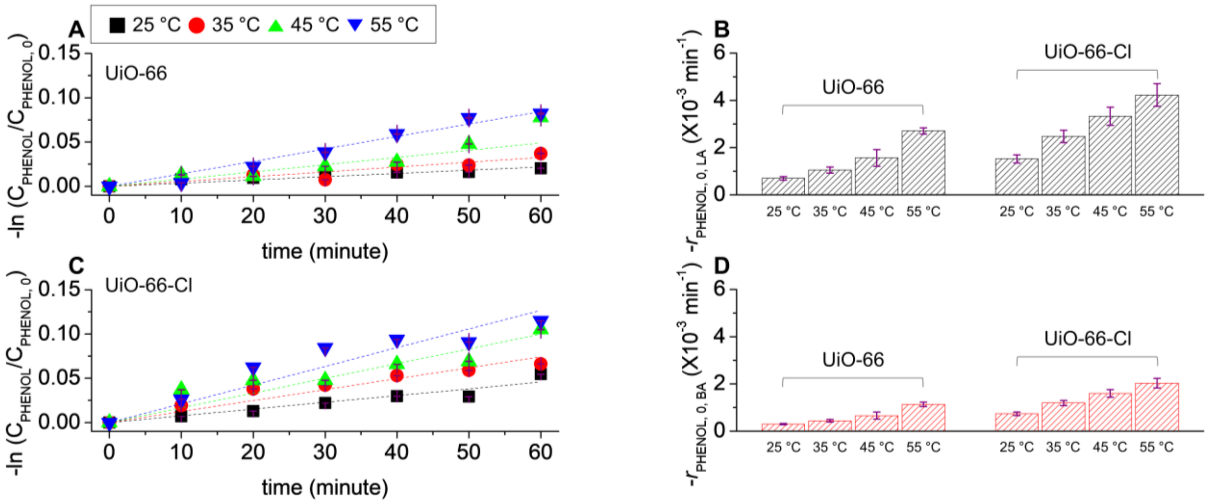

Fig. S21. Fittings of background-subtracted reaction data to pseudo-1st-order kinetic model (-ln ($C_{PHENOL}/C_{PHENOL, 0}$) versus time) for assessing apparent reaction rate constants (k_{APP} values in Table S12) of UiO-66 (A)/UiO-66-Cl (C) in degrading phenol with the variation of reaction temperatures (25-55 °C). In (A) and (C), background denotes phenol degradation mediated by H_2O_2 self-dissection (in the absence of UiO-66/UiO-66-Cl) or phenol adsorption on UiO-66 or UiO-66-Cl surface (in the absence of H_2O_2) under the reaction environments specified below. $C_{PHENOL, 0}$ and C_{PHENOL} indicate phenol concentration initially fed and phenol concentration present in reaction mixture at a specific reaction time, respectively. Plots of '25 °C' ('without scavenger' in Fig. S19) were re-plotted for comparison. Background-subtracted initial phenol degradation rates of UiO-66 or UiO-66-Cl in a per-LA site basis or in a per-BA site basis at 25-55 °C: $-r_{PHENOL, 0, LA}$ for (B) and $-r_{PHENOL, 0, BA}$ for (D). Reaction conditions: 0.2 g of UiO-66 (or UiO-66-Cl) with sizes of <60 µm; 30 mmol of H_2O_2; 0.1 mmol of phenol; 100 mL of de-ionized H_2O; initial pH of 7.0; 25-55 °C; 300 rpm.

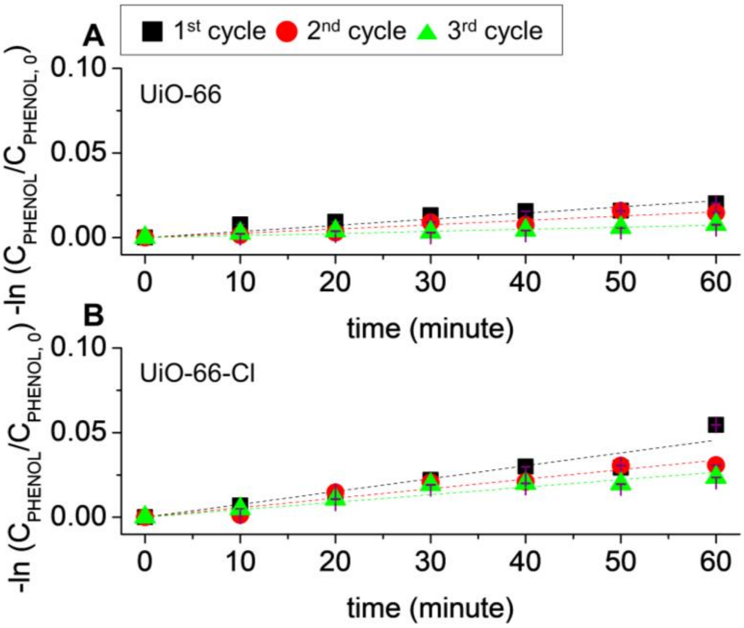

Fig. S22. Fittings of background-subtracted reaction data to pseudo-1st-order kinetic model (-ln ($C_{PHENOL}/C_{PHENOL,\,0}$) versus time) for assessing apparent reaction rate constants (k_{APP} values in Table S12) of UiO-66 (A)/UiO-66-Cl (B) in degrading phenol (as-synthesized for the 1st cycle; used for the 2nd-3rd cycles). In (A-B), background denotes phenol degradation mediated by H_2O_2 self-dissection (in the absence of UiO-66/UiO-66-Cl) or phenol adsorption on UiO-66 or UiO-66-Cl surface (in the absence of H_2O_2) under the reaction environments specified below. $C_{PHENOL,\,0}$ and C_{PHENOL} indicate phenol concentration initially fed and phenol concentration present in reaction mixture at a specific reaction time, respectively. Plots of '1st cycle' ('without scavenger' in Fig. S19) were re-plotted for comparison. Reaction conditions: 0.2 g of UiO-66 (or UiO-66-Cl) as-synthesized or used with sizes of <60 µm; 30 mmol of H_2O_2; 0.1 mmol of phenol; 100 mL of de-ionized H_2O; initial pH of 7.0; 25 °C; 300 rpm.

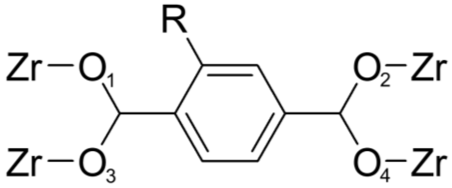

Fig. S23. MOF architectures simplified for DFT calculations, where R denotes H (for UiO-66) or Cl_{SUP}/Cl^{-}_{SUP}/$Cl^{\bullet}_{SUP}$ (for UiO-66-Cl).

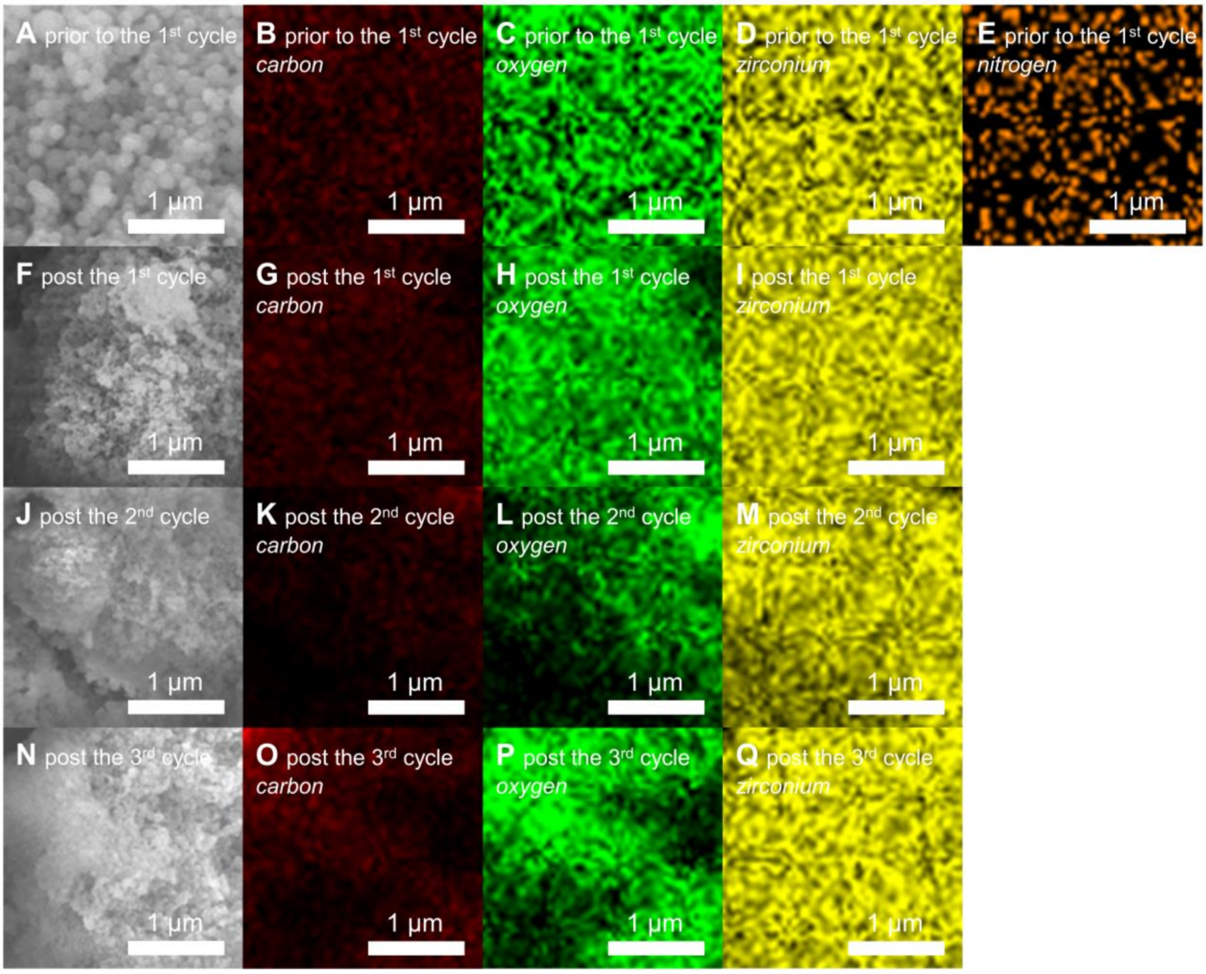

Fig. S24. SEM (A, F, J, and N) and EDX mapping images of UiO-66 prior to or post phenol degradation recycle runs (B-E for prior to the 1st cycle; G-I for post the 1st cycle; K-M for post the 2nd cycle; O-Q for post the 3rd cycle).

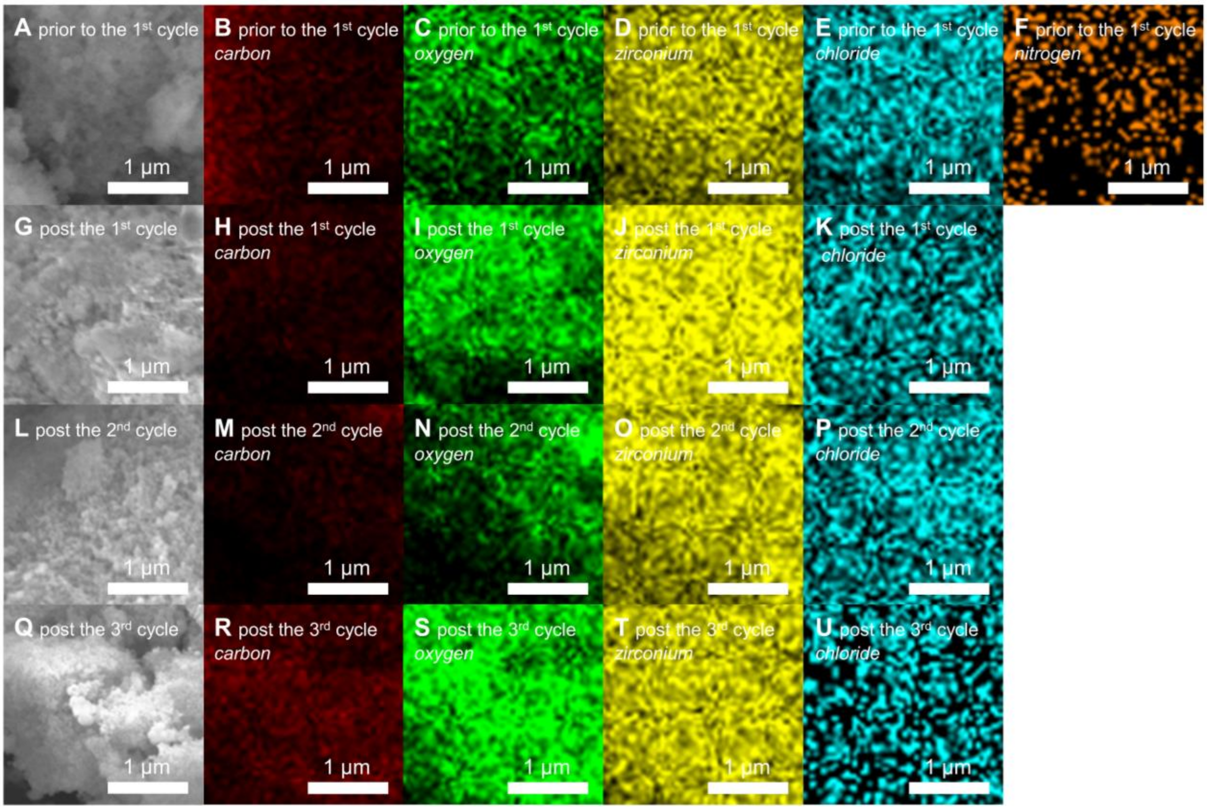

Fig. S25. SEM (A, G, L, and Q) and EDX mapping images of UiO-66-Cl prior to or post phenol degradation recycle runs (B-F for prior to the 1st cycle; H-K for post the 1st cycle; M-P for post the 2nd cycle; R-U for post the 3rd cycle).

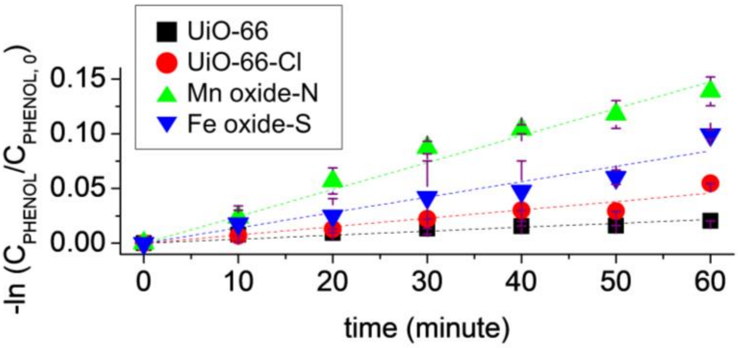

Fig. S26. Fittings of background-subtracted reaction data to pseudo-1st-order kinetic model (-ln ($C_{PHENOL}/C_{PHENOL, 0}$) versus time) for assessing apparent reaction rate constants (k_{APP} values in Table S12) of UiO-66, UIO-66-Cl, Mn oxide-N, and Fe oxide-S in degrading phenol. Background denotes phenol degradation mediated by H_2O_2 self-dissection (in the absence of the material) or phenol adsorption on the material surface (in the absence of H_2O_2) under the reaction environments specified below. $C_{PHENOL, 0}$ and C_{PHENOL} indicate phenol concentration initially fed and phenol concentration present in reaction mixture at a specific reaction time, respectively. Plots of 'UiO-66/UiO-66-Cl' ('without scavenger' in Fig. S19) were re-plotted for comparison. Reaction conditions: 0.2 g of the material with sizes of <60 µm; 30 mmol of H_2O_2; 0.1 mmol of phenol; 100 mL of de-ionized H_2O; initial pH of 7.0; 25 °C; 300 rpm.

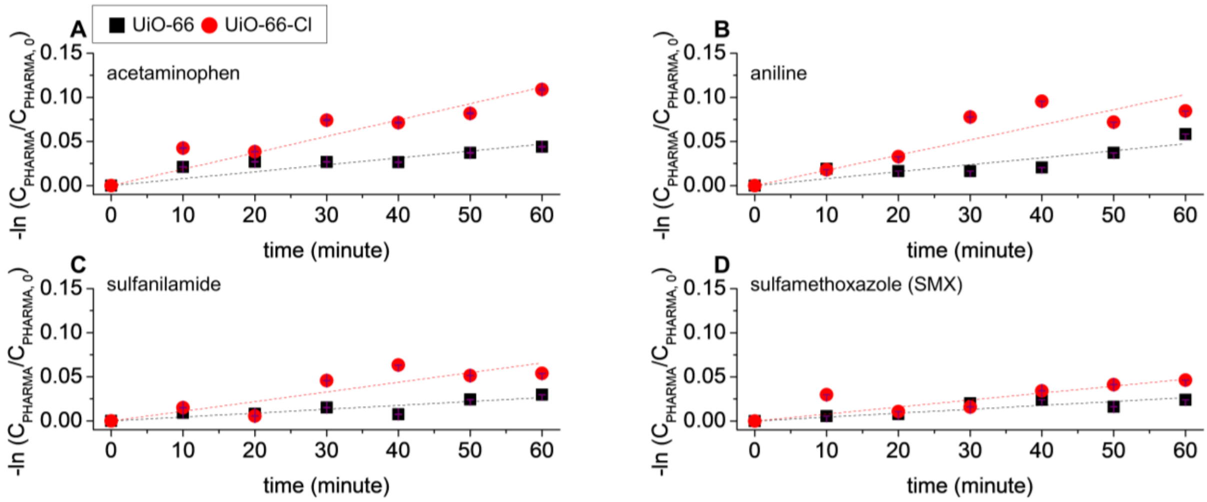

Fig. S27. Fittings of background-subtracted reaction data to pseudo-1st-order kinetic model (-ln ($C_{XXX}/C_{XXX,\,0}$) versus time; XXX denotes acetaminophen (A), aniline (B), sulfanilamide (C), or sulfamethoxazole (SMX; D)) for assessing apparent reaction rate constants (k_{APP} values in Table S12) of UiO-66 and UIO-66-Cl in degrading aniline or pharmaceutical compounds. Background denotes aniline (or pharmaceutical compound) degradation mediated by H_2O_2 self-dissection (in the absence of UiO-66/UiO-66-Cl) or aniline (or pharmaceutical compound) adsorption on UiO-66 or UiO-66 surface (in the absence of H_2O_2) under the reaction environments specified below. $C_{PHARMA,\,0}$ and C_{PHARMA} indicate the concentration of aniline (or pharmaceutical compound) initially fed and that present in reaction mixture at a specific reaction time, respectively. Reaction conditions: 0.2 g of UiO-66 (or UiO-66-Cl) with sizes of <60 µm; 30 mmol of H_2O_2; 0.007 mmol of acetaminophen, aniline, sulfanilamide, or SMX; 100 mL of de-ionized H_2O; initial pH of 7.0; 25 °C; 300 rpm.

References

1. M. Lammert, S. Bernt, F. Vermoortele, D. E. De Vos and N. Stock, *Inorg. Chem.*, 2013, **52**, 8521-8528.
2. J. Jacobsen, L. Wegner, H. Reinsch and N. Stock, *Dalton Trans.*, 2020, **49**, 11396-11402.
3. S. T. Meek, J. J. Perry, S. L. Teich-McGoldrick, J. A. Greathouse and M. D. Allendorf, *Cryst. Growth Des.*, 2011, **11**, 4309-4312.
4. G. Cai and H.-L. Jiang, *Angew. Chem. Int. Ed.*, 2017, **56**, 563-567.
5. S. He, Y. Chen, Z. Zhang, B. Ni, W. He and X. Wang, *Chem. Sci.*, 2016, **7**, 7101-7105.
6. . Kim, J. Park, S. H. Kim, J.-H. Lee, K. Jeong and J. Kim, *Carbon*, 2023, **203**, 630-649.
7. J. Kim, S. Lee and H. P. Ha, *ACS Catal.*, 2021, **11**, 767-786.
8. J. Kim, Y. J. Choe, S. H. Kim, I.-S. Choi and K. Jeong, *JACS Au*, 2021, **1**, 1158-1177.
9. J. Kim, Y. J. Choe, S. H. Kim and K. Jeong, *Appl. Catal. B*, 2019, **252**, 62-76.
10. J. Kim, Y. J. Choe, S. H. Kim, S.-C. Lee and S. Bhattacharjee, *Appl. Catal. B*, 2019, **253**, 60-68.
11. S. Lee, J.-H. Lee, H. P. Ha and J. Kim, *Chem. Mater.*, 2022, **34**, 1078-1097.
12. J. Kim, Y. J. Choe and S. H. Kim, *Chem. Eng. J.*, 2021, **413**, 127550.
13. D. H. Kim, S.-H. Oh, H. P. Ha, Y.-C. Joo and J. Kim, *Appl. Surf. Sci.*, 2023, **614**, 156099.
14. Y. J. Choe, S. H. Kim, K. Jeong and J. Kim, *Chem. Eng. J.*, 2023, **455**, 140537.
15. N. Tannert, S. Gökpinar, E. Hastürk, S. Nießing and C. Janiak, *Dalton Trans.*, 2018, **47**, 9850-9860.
16. G. C. Shearer, S. Chavan, S. Bordiga, S. Svelle, U. Olsbye and K. P. Lillerud, *Chem. Mater.*, 2016, **28**, 3749-3761.
17. J. Kim, A. G. Oliver and J. C. Hicks, *CrystEngComm*, 2015, **17**, 8015-8020.
18. R. C. Klet, Y. Liu, T. C. Wang, J. T. Hupp and O. K. Farha, *J. Mater. Chem. A*, 2016, **4**, 1479-1485.
19. M. J. Frisch, G. W. Trucks, H. B. Schlegel, G. E. Scuseria, M. A. Robb, J. R. Cheeseman, G. Scalmani, V. Barone, G. A. Petersson, H. Nakatsuji, X. Li, M. Caricato, A. V. Marenich, J. Bloino, B. G. Janesko, R. Gomperts, B. Mennucci, H. P. Hratchian, J. V. Ortiz, A. F. Izmaylov, J. L. Sonnenberg, Williams, F. Ding, F. Lipparini, F. Egidi, J. Goings, B. Peng, A. Petrone, T. Henderson, D. Ranasinghe, V. G. Zakrzewski, J. Gao, N. Rega, G. Zheng, W. Liang, M. Hada, M. Ehara, K. Toyota, R. Fukuda, J. Hasegawa, M. Ishida, T. Nakajima, Y. Honda, O. Kitao, H. Nakai, T. Vreven, K. Throssell, J. A. Montgomery Jr., J. E. Peralta, F. Ogliaro, M. J. Bearpark, J. J. Heyd, E. N. Brothers, K. N. Kudin, V. N. Staroverov, T. A. Keith, R. Kobayashi, J. Normand, K. Raghavachari, A. P. Rendell, J. C. Burant, S. S. Iyengar, J. Tomasi, M. Cossi, J. M. Millam, M. Klene, C. Adamo, R. Cammi, J. W. Ochterski, R. L. Martin, K. Morokuma, O. Farkas, J. B. Foresman and D. J. Fox, *Gaussian, Inc.,Wallingford CT*,2016.
20. Y. Zhao and D. G. Truhlar, *J. Chem. Phys.*, 2006, **125**, 194101.
21. J. E. Mondloch, M. J. Katz, W. C. Isley Iii, P. Ghosh, P. Liao, W. Bury, G. W. Wagner, M. G. Hall, J. B. DeCoste, G. W. Peterson, R. Q. Snurr, C. J. Cramer, J. T. Hupp and O. K. Farha, *Nat. Mater.*, 2015, **14**, 512-516.
22. S. Luo, B. Averkiev, K. R. Yang, X. Xu and D. G. Truhlar, *J. Chem. Theory Comput.*, 2014, **10**, 102-121.
23. F. Weigend and R. Ahlrichs, *Phys. Chem. Chem. Phys.*, 2005, **7**, 3297-3305.
24. J. M. L. Martin and A. Sundermann, *J. Chem. Phys.*, 2001, **114**, 3408-3420.
25. A. V. Marenich, C. J. Cramer and D. G. Truhlar, *J. Phys. Chem. B*, 2009, **113**, 6378-6396.
26. D. Minakata, W. Song and J. Crittenden, *Environ. Sci. Technol.*, 2011, **45**, 6057-6065.
27. H.-H. Kim, J. Y. Seo, H. Kim, S. Jeong, K.-Y. Baek, J. Kim, S. Min, S. H. Kim and K. Jeong, *ACS Appl. Mater. Interfaces*, 2021, **13**, 3782-3792.
28. A. S. Menon and L. Radom, *J. Phys. Chem. A*, 2008, **112**, 13225-13230.
29. R. Kaur and Vikas, *RSC Adv.*, 2016, **6**, 29080-29098.
30. Y. J. Choe, J.-S. Kim, H. Kim and J. Kim, *Chem. Eng. J.*, 2020, **400**, 125971.
31. M. Kim, S. H. Kim, J.-H. Lee and J. Kim, *J. Hazard. Mater.*, 2020, **392**, 122347.
32. S. S. Shinde, M. P. Hay, A. V. Patterson, W. A. Denny and R. F. Anderson, *J. Am. Chem. Soc.*, 2009, **131**, 14220-14221.
33. S. Dikalov, J. Jiang and R. P. Mason, *Free Radic. Res.*, 2005, **39**, 825-836.
34. J. M. Fontmorin, R. C. Burgos Castillo, W. Z. Tang and M. Sillanpää, *Water Res.*, 2016, **99**, 24-32.
35. C. Bernofsky, B. M. R. Bandara and O. Hinojosa, *Free Radic. Biol. Med.*, 1990, **8**, 231-239.